UNIVERSITY OF HELSINKI
DEPARTMENT OF PHYSICS

REPORT SERIES IN GEOPHYSICS

No 58

OBSERVATIONS OF ATMOSPHERIC BOUNDARY LAYER OVER SEA ICE IN A SVALBARD FJORD

Eeva Mäkiranta

HELSINKI 2009

UNIVERSITY OF HELSINKI
DEPARTMENT OF PHYSICS

REPORT SERIES IN GEOPHYSICS

No 58

OBSERVATIONS OF ATMOSPHERIC BOUNDARY LAYER OVER SEA ICE IN A SVALBARD FJORD

Eeva Mäkiranta

HELSINKI 2009

Abstract

Sonic anemometer and profile measurements made in Wahlenbergfjorden, Svalbard, in 2006 and 2007 were used to study the conditions in the atmospheric boundary layer over sea ice. The aim was to study turbulent fluxes by applying the Monin-Obukhov similarity theory and to investigate the effects of topography and mesoscale phenomena on the surface layer.

The turbulent surface fluxes of momentum and sensible heat were calculated using the eddy correlation method and the gradient method. The gradient method systematically gave larger fluxes than the eddy correlation method. Large uncertainties in flux estimates were mostly related to meteorological problems and limited resolution of the instruments when measuring small fluxes. Plots of the measurement based similarity functions against stability parameter showed that the theoretical universal similarity functions underestimated turbulent mixing. Validity of the Monin-Obukhov similarity theory proved to be essential for the results, but it was questionable for cross-fjord wind directions and in the presence of mesoscale variability or topographic effects. In these cases the requirements of horizontal homogeneity and stationarity were not fulfilled. Local conditions such as surface roughness showed spatial variations and a dependence on wind direction. The roughness length values were on the order of 10^{-3} to $10^{-4}m$, which are typical values for snow-covered ice. The roughness lengths for along-fjord wind directions were smaller than those for cross-fjord directions.

The results were found to be essentially affected by the synoptic situation. However, the data also revealed the existence of topographic and mesoscale effects. Both channelling effects and drainage flows likely occurred. Mesoscale variability proved to be weaker in case of a strong mean flow.

Contents

1 Introduction

The atmospheric boundary layer is the portion of the atmosphere closest to the Earth's surface. At mid-latitudes the boundary layer thickness is typically from one kilometer to a few kilometers, while in the Arctic the boundary layer is more shallow, a few hundred meters or less. Within the boundary layer the flow is dominated by turbulence. The turbulent exchange of heat, momentum and moisture at the surface is directly influenced by the meteorological and dynamical properties of the boundary layer. On the other hand, the surface fluxes of momentum, heat and moisture are very important because of their strong influence on the mean profiles in the lower atmosphere. The Monin-Obukhov similarity theory (Monin and Obukhov, 1954) has been widely used to describe mean wind speed, temperature and moisture as a function of height in the surface layer, which is the lowest layer of the atmospheric boundary layer. Within the surface layer the turbulent fluxes are assumed to be constant with height. Traditionally, turbulent fluxes are derived from vertical wind speed and temperature profiles. The effects of stability are accounted for with universal functions, which result from the application of the Monin-Obukhov similarity theory, but have to be determined empirically. The effects of stability vanish in neutral conditions and the profiles become semilogarithmic.

The interaction between atmosphere and surface is particularly complex in the case of a heterogeneous surface, such as fractured sea ice. If the ice is fractured by leads, for example, the heat fluxes from the leads modify the stability and characteristics of the atmospheric boundary layer.

Exchange processes in Arctic regions have been studied in several field experiments. These include the SHEBA (Surface Heat Budget of the Arctic Ocean Experiment) measurement program from 1997 to 1998, during which a comprehensive set of atmospheric measurements was collected (Uttal et al., 2002), and the ARTIST (Arctic Radiation and Turbulence Interaction Study) experiment, which was conducted in Svalbard in the spring of 1998 (Hartmann et al., 1999).

These studies have shown that the arctic boundary layer is usually stably stratified during the winter and neutral or only weakly stratified during the summer.

The climate of Svalbard is strongly influenced by the atmospheric general circulation, the annual variation in light conditions, sea ice extent and ocean currents (Svendsen et al., 2002). The synoptic scale weather conditions (wind speed, air-surface temperature difference, cloud fields) primarily cause the variability of turbulent and radiative fluxes. The synoptically caused variability is modified by the local conditions such as fetch, roughness or ice thickness (Brümmer et al., 2002). Turbulent transport of energy and momentum in the atmospheric boundary layer depends strongly on the sea ice characteristics, such as concentration (lead cover), thickness, surface topography and snow thickness. In addition, the low-level circulation over Svalbard fjords is strongly influenced by the orography and winds of local origin such as katabatic winds. These winds transport cold and heavy air from inland glaciers to the warmer sea, which can modify the boundary layer structure (Argentini et al., 2003).

During UNIS (the University Centre in Svalbard) scientific cruises, a wide range of meteorological data have been collected in various locations in the Svalbard area. The data have been collected with slow-response profile instruments, fast-response instruments (sonic anemometers), radiation instruments and tethered balloons. These data are complemented with some data on ice and snow properties and some oceanographic data. In this study, some of the data will be analyzed to study the characteristics of the atmospheric boundary layer. The main focus will be on measurements conducted on land-fast sea ice in Wahlenbergfjorden (Figure 4.2) in the spring of 2006 and 2007. The spatial variability and effects of topography will be investigated. Turbulent fluxes of heat and momentum will be calculated and compared using different methods, such as the eddy correlation method and the gradient method. In order to derive the turbulent fluxes, use will be made of the Monin-Obukhov similarity theory. Possible error sources will be considered and data quality assessed. The validity of the Monin-Obukhov similarity theory will also be discussed.

In Chapter 2, some general characteristics of atmospheric boundary layer are described. Chapter 3 presents some observations of the boundary layer from previous studies. A description of the measurement site and instrumentation is given in Chapter 4. The methods used are presented in Chapter 5. The results of the measurements are presented in Chapter 6 and discussed in Chapter 7. Conclusions are summarized in Chapter 8.

2 Boundary layer theory

2.1 Definition of a boundary layer

The atmospheric boundary layer can be defined as the part of the troposphere that is directly influenced by the presence of the Earth's surface, and responds to changes in surface forcings on a timescale of an hour or less (Stull, 1988). These forcings include frictional drag, evaporation and transpiration, processes affecting the transfer of heat, momentum and moisture, pollutant emission, and terrain induced flow modification. The boundary layer thickness varies in time and space, ranging from tens of meters in strongly stable situations to a few kilometers in convective conditions. Diurnal variation is one of the key characteristics of the boundary layer over land, while the free atmosphere shows little diurnal variation. The ground warms and cools in response to solar radiation, which in turn forces changes in the boundary layer via transport processes. Turbulence is one of the important transport processes, and is sometimes also used to define the boundary layer (Stull, 1988).

2.2 Turbulence

Even though turbulence is a rather familiar notion, it is not easy to define precisely. Some of the general characteristics of turbulence include (Arya, 2001):

1. irregularity or randomness
2. three-dimensionality and rotationality
3. diffusivity or ability to mix properties
4. dissipativeness
5. multiplicity of scales of motion

In a turbulent flow, variables fluctuate irregularly in time and space. There-

fore, a common approach for studying turbulence is to split variables into a mean part and a perturbation part. Thus, any variable A can be separated into a component $\overline{A}$, defining average conditions over a specific averaging period, and a component a' that denotes the deviation from the average. To make sure that a physically reasonable separation of underlying processes is performed, the corresponding averaging period has to be selected very carefully.

To study and describe the turbulence structure, we have to deal with statistical approaches. The simplest measures of fluctuation levels are the variances ($\overline{u'^2}$, $\overline{v'^2}$, $\overline{w'^2}$, $\overline{\theta'^2}$, etc.), defined as the average of the square of the turbulent part of a variable, and standard deviations ($\sigma_u = (\overline{u'^2})^{(1/2)}$, etc.), defined as the square root of the variance. Even more important are the covariances ($\overline{u'w'}$, $\overline{v'w'}$, $\overline{\theta'w'}$, etc.), which are directly related to turbulent fluxes of momentum, heat, etc. Covariances are averages of products of two fluctuating variables and depend on the correlations between these variables.

2.3 Stability

Atmospheric stability describes how easily an air parcel can move vertically in the atmosphere and it depends on the vertical temperature structure. There are three cases of stability; unstable (convective), stable and neutral.

One widely used measure of stability is the Richardson number, which is a dimensionless ratio between buoyancy forces and velocity shears. There are several different definitions of this, including the gradient, flux and bulk Richardson numbers. The gradient Richardson number is defined as

$$Ri = \frac{g\frac{\partial\overline{\theta}}{\partial z}}{\theta_0(\frac{\partial\overline{u}}{\partial z})^2} \tag{2.1}$$

where g is the acceleration due to gravity, θ_0 potential temperature in the surface layer, z the observation height, $\overline{\theta}$ the mean potential temperature and $\overline{u}$ the mean wind speed. Assuming a dry adiabatic lapse rate in the atmosphere, potential temperature θ can be approximated as $\theta \cong T + 0.0098z$ where T is the temperature measured at a level z. The Richardson number is positive for stable stratification, negative for unstable stratification and zero for neutral stratification. In stable conditions, turbulence is presumed to cease as the Richardson number exceeds a critical value, which is traditionally assumed to be 0.2-0.25. One advantage in

using the Richardson number is that it contains gradients of mean quantities that are easy to measure. However, it is an unknown function of height and cannot be used for characterising surface layer structure in the vertical direction.

Another commonly used measure of stability is the stability parameter $\zeta = z/L$, defined as the ratio of the reference height z and the Obukhov length

$$L = -\frac{u_*^3 \theta_v}{kg\overline{w'\theta_v'}} \tag{2.2}$$

where $u_* = \sqrt{(-\overline{u'w'})^2 + (-\overline{v'w'})^2}$ is the friction velocity, k the von Kármán constant, θ_v the mean virtual potential temperature of the layer and $\overline{w'\theta_v'}$ the turbulent vertical flux of virtual potential temperature. One physical interpretation of the Obukhov length is that it is proportional to the height above the surface at which the buoyancy factors become dominant over mechanical production of turbulence (Stull, 1988).

The Richardson number and the stability parameter $\zeta = z/L$ have the same sign and they can be assumed to be related as

$$z/L = Ri \qquad \text{for } Ri < 0 \tag{2.3}$$

and

$$z/L = \frac{Ri}{1 - 5Ri} \qquad \text{for } 0 < Ri < 0.2. \tag{2.4}$$

2.4 The Monin-Obukhov similarity theory

The Monin-Obukhov similarity theory (Monin and Obukhov, 1954) relates the profiles of wind speed, potential temperature and humidity to the surface fluxes of momentum, sensible heat (heat that results in a temperature change) and moisture. The theory is usually applied to the surface layer and is sometimes referred to as surface-layer similarity theory. The surface layer is the lowest part of the boundary layer where fluxes vary by less than 10% of their magnitude with height. We can thus assume that the fluxes are constant with height in the surface layer. This is one of the basic assumptions of the Monin-Obukhov similarity theory. The theory also assumes horizontal homogeneity and stationarity, and it is only applicable when the winds are not calm and u_* is not zero. The molecular exchange should be small compared to turbulent exchange.

The theory is based on the assumption that the structure of turbulence is determined by a few key parameters; the height above the surface z, the buoyancy parameter g/θ, the friction velocity u_* and the surface potential temperature flux $\overline{w'\theta'}$. According to the theory, various atmospheric parameters and statistics, such as gradients, variances and covariances, when properly scaled, become universal functions of the stability parameter $\zeta = z/L$.

The non-dimensional vertical gradients of mean wind speed ($\overline{U}$) and potential temperature ($\overline{\theta}$) are assumed to be

$$\frac{kz}{u_*}\frac{\partial \overline{U}}{\partial z} = \phi_m(\zeta) \tag{2.5}$$

$$\frac{kz}{\theta_*}\frac{\partial \overline{\theta}}{\partial z} = \phi_h(\zeta) \tag{2.6}$$

where $\theta_* = -\overline{w'\theta'}/u_*$ is the temperature scale based on the surface potential temperature flux and $\phi_m(\zeta)$ and $\phi_h(\zeta)$ are non-dimensional universal similarity functions for velocity and potential temperature gradient, respectively. Commonly the von Kármán constant k is determined such that in neutral conditions, the gradient similarity functions are unity. In this study, the traditional value of $k = 0.4$ is used for both wind speed and temperature profiles.

2.4.1 Empirical forms of similarity functions

The exact forms of similarity functions are not predicted by the Monin-Obukhov similarity theory and therefore have to be determined empirically. A number of micrometeorological field experiments have been conducted in order to verify the Monin-Obukhov similarity theory and to determine the forms of the similarity functions. Based on these experiments, various forms for ϕ_m and ϕ_h have been suggested (Businger et al., 1971; Holtslag and De Bruin, 1988; Högström, 1988; Beljaars and Holtslag, 1991). The so-called Businger-Dyer relations are widely used in unstable cases (Businger et al., 1971; Paulson, 1970):

$$\phi_m^2(\zeta) = \phi_h(\zeta) = (1 - 16\zeta)^{(-1/2)} \qquad \text{for } \zeta < 0 \text{ (unstable)} \tag{2.7}$$

Figure 2.1 presents these Businger-Dyer relations for unstable regions. In this study, the Businger-Dyer forms were used for unstable situations.

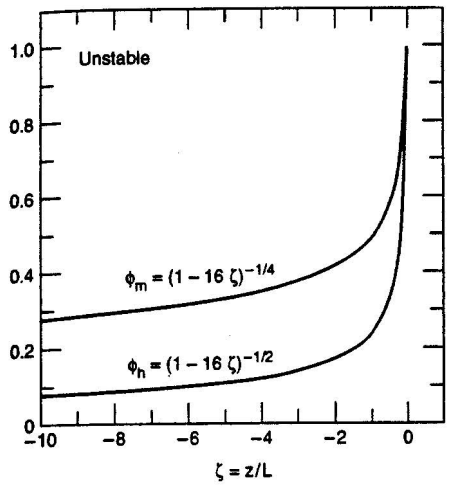

Figure 2.1: *Forms of similarity functions in unstable situations (Andreas, 1998).*

Stable and especially very stable cases are not as well studied as the unstable cases, and the stability functions differ considerably between different studies. Some of the suggested stability functions are presented in Figure 2.2. In this study, the expressions suggested by Holtslag and De Bruin (1988) were adopted for stable regions:

$$\phi_m = \phi_h = 1 + 0.7\zeta + 0.75\zeta(6 - 0.35\zeta)exp(-0.35\zeta) \tag{2.8}$$

.

These expressions are specially adapted for treating very stable stratification and are recommended by Andreas (2002) for representing stratification effects for surface-layer wind speed, temperature and humidity profiles in all stable situations. They are especially recommended for describing stable stratification over snow and ice.

The similarity relations $\phi_m(\zeta)$ and $\phi_h(\zeta)$ can be integrated with height to yield the corresponding profile functions $\psi_m(\zeta)$ and $\psi_h(\zeta)$. The integrated forms used for stable stratification in this study can be written as (Holtslag and De Bruin, 1988):

$$\psi_m = \psi_h = -0.7\zeta + 0.75(\zeta - \frac{5}{0.35})exp(0.35\zeta) + \frac{3.75}{0.35} \tag{2.9}$$

For unstable regions the integrated forms can be expressed as (e.g. Paulson, 1970):

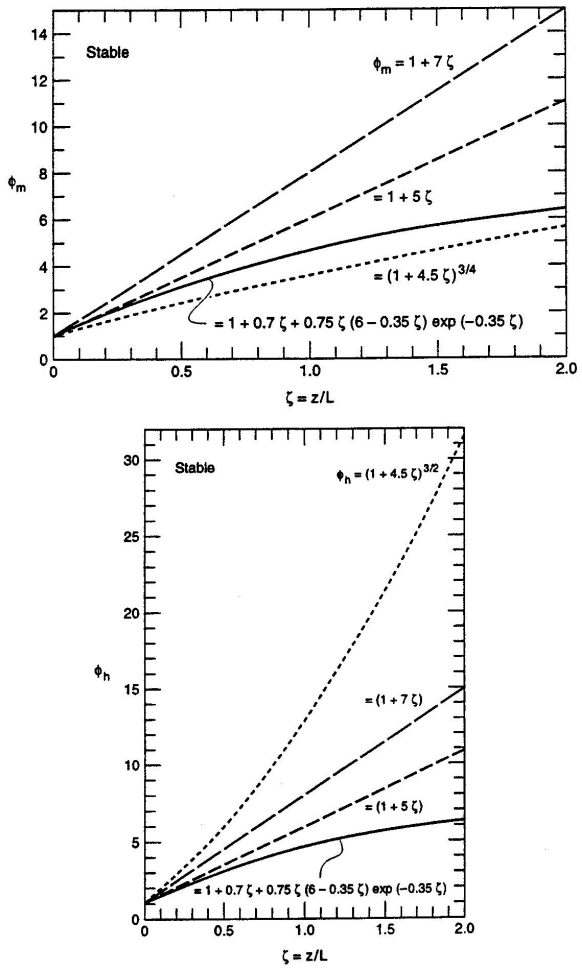

Figure 2.2: *Forms of similarity functions in stable situations (Andreas, 1998).*

$$\psi_m = 2ln[\frac{1+X}{2}] + ln[\frac{1+X^2}{2}] + \frac{\pi}{2} - 2tan^{-1}X \tag{2.10}$$

$$\psi_h = 2ln[\frac{1+Y}{2}] \tag{2.11}$$

where $X = \phi_m^{-1} = (1 - 16\zeta)^{1/4}$ and $Y = \phi_h^{-1} = (1 - 16\zeta)^{1/2}$.

2.5 Channelling and drainage flows in the atmospheric boundary layer

Channelling refers to the funnelling of winds resulting from topographic features. It causes changes in the direction of prevailing winds and/or in wind speeds. Channelling can be divided into forced channelling and pressure-driven channelling

(Whiteman, 2000). Forced channelling occurs when upper winds are brought down into a valley and turned to flow along the valleys longitudinal axis. Pressure-driven channelling, on the other hand, is caused by strong horizontal pressure gradient across a gap, channel or pass. Forced channelling of large-scale winds is strongest when winds aloft blow parallel to the valley axis, while pressure-driven channelling is strongest when the along-valley pressure gradient is strongest (Whiteman, 2000).

Drainage flows are katabatic winds that occur when cold, dense air moves downslope under the influence of gravity. Drainage flows can be generated on slopes as low as 1 % or even less. The scale of katabatic winds varies from large-scale flows on the ice sheets of Antarctica and Greenland to small-scale flows in valleys or on glaciers. The depth of a downslope wind varies over time and space. The depth increases with distance down the slope and it can be approximated to be about 5 % of the drop in elevation (Whiteman, 2000). Strong stability or an inversion tend to decrease the downslope flow depth. Near the ground, drag reduces the wind speed. There is a wind maximum above the ground, the height of which has been found to depend on the stability (Van Der Avoird and Duynkerke, 1999). Apart from the wind maximum, the katabatically forced boundary layer can be expected to have a similar structure to a stable, nocturnal boundary layer over a flat surface. Drainage flows are not always cold, since the air experiences adiabatic warming as it descends. Drainage flows can also mix the stably stratified boundary layer, thus causing a warming effect. When mean winds are light, drainage flows in the same direction as the mean flow are enhanced, while drainage flows in the opposing direction are reduced. Strong mean winds completely suppress the opposed slope winds (Stull, 1988).

Channelling and drainage winds may also occur simultaneously. These situations are often characterised by high wind speeds.

3 Observations of the boundary layer

3.1 Boundary layer structure

Over oceans, the large heat capacity of water combined with tremendous mixing within the top of the ocean cause a slowly varying sea surface temperature. Thus, the atmospheric boundary layer depth varies relatively slowly in time and space. Over both land and ocean, the boundary layer tends to be thinner in high-pressure regions than in low-pressure regions. Over land in high pressure regions the boundary layer has a well defined structure that evolves with the diurnal cycle. It consists of three major parts: the mixed layer (convective layer), the residual layer and the stable boundary layer (Stull, 1988). The mixed layer grows during daytime due to solar heating of the ground. Turbulence in the mixed layer is usually convectively driven and causes heat, momentum and moisture to be uniformly mixed vertically. The residual layer is formed when turbulence decays in the mixed layer after sunset. The residual layer is neutrally stratified. It is not in direct contact with the ground since it lies on top of the stable boundary layer. The stable boundary layer modifies the bottom of the residual layer, but the rest of the residual layer is not affected by turbulent transport from the surface and thus does not follow the exact definition of a boundary layer (Stull, 1988). Nevertheless, the whole residual layer is often included in boundary layer studies. The stable boundary layer forms during the night and is characterised by statically stable air and weak, sporadic turbulence. The winds are lighter or calm, but nocturnal low-level jets or gravity-driven drainage winds may occur. Also wave motions are frequent.

The surface layer is the region at the bottom of the boundary layer where turbulent fluxes and stress vary by less than 10 % of their magnitude. Thus, the bottom of the boundary layer is called the surface layer, regardless of whether it

is part of a mixed layer or stable boundary layer (Stull, 1988).

3.2 Boundary layer over Arctic sea ice

Sea ice is a special surface type. It consists of ice floes of varying thickness and is fractured by cracks, leads and polynyas or it can be fast ice close to shore (Vihma, 2005). Fractured sea ice with ice floes of different size and distribution is quite an inhomogeneous surface, which makes the interaction between atmosphere and surface particularly complex (Brümmer et al., 2002). The Arctic pack ice, however, can be a rather uniform and homogeneous surface with almost unlimited and extremely uniform fetch (Grachev et al., 2007). The sea ice and its snow cover act as insulators between the relatively warm ocean and cold atmosphere, and the vertical temperature gradient through the ice and snow layer is large.

The knowledge of the boundary layer over Arctic sea ice is based on observations made from drifting stations (e.g. Jordan et al., 1999; Persson et al., 2002; Grachev et al., 2007), airborne measurements (e.g. Hartmann et al., 1999; Brümmer and Thiemann, 2002), ships and coastal stations. On the basis of the data from the Arctic, the wintertime atmospheric surface layer over thick sea ice is typically stably stratified. The stable boundary layer can be formed by radiative cooling of the surface or by advection of warmer air from the ocean over the ice. Our knowledge of the stably stratified boundary layer is mostly based on observations of the mid-latitude nocturnal stable boundary layer (Vihma, 2005). In polar regions, however, the low sun angle, the high reflectivity and emissivity of the snow surface and the long polar nights allow the stable boundary layer to develop and reach a steady state. As a result, the stable boundary layer can last for several days and have a more complicated structure. Also ground inversions are frequent and may be very strong and long-lasting (Serreze et al., 1992; Persson et al., 2002). Diurnal variations are weak or not present at all, but seasonal variation in the boundary layer structure is large. Turbulence in the polar stable boundary layer is usually weak or intermittent.

The boundary layer shows more variation over the marginal ice zone, where the sea ice is more fractured and the ice edge is diffuse. The boundary layer structure depends strongly on the wind direction relative to the ice edge. When the flow crosses the ice edge, an internal boundary layer develops. The air mass modification is different in case of an on-ice flow (e.g. Brümmer and Thiemann, 2002; Vihma et al., 2003) and an off-ice flow (e.g. Olsson and Harrington, 2000).

Winds are the primary driving force of ice motion and the changes in surface roughness play an important role in the wind forcing of sea ice drift. The momentum flux acts like a stress on sea ice. The strength of exchange of momentum is described by the atmospheric drag coefficient which is dependent on the surface roughness and stratification. Irregular terrain affects the low-level flow by a surface drag. The total surface drag can be divided into skin drag and form drag. Form drag is mainly caused by ice ridges. Drifting and blowing snow is an important factor in setting the drag properties of snow-covered sea ice (Andreas et al., 2005).

The turbulent sensible heat flux is driven by a difference in temperature between the surface and the air. Over Arctic sea ice, it is often directed downward due to radiative cooling of the surface. The snow and ice surfaces are highly reflective for shortwave radiation and heat is effectively lost in the form of longwave radiation into the overlying atmosphere. The surface is generally colder than the air and the turbulent sensible heat flux is directed toward the surface. The turbulent flux of latent heat is generally small due to small absolute moisture content at low temperatures.

4 Site and instrumentation

4.1 Measurement site

Measurements of the atmospheric boundary layer were done as a part of UNIS fieldwork campaigns on land-fast sea ice in Wahlenbergfjorden, a fjord in the western part of Nordaustlandet, Svalbard (see Figures 4.1 and 4.2). It is oriented from west to east and opens up to Hinlopenstretet, which is a strait separating the islands of Nordaustlandet and Spitsbergen. Wahlenbergfjorden is situated between 79°49' and 79°37'N and 18°47' and 21°52'E. It is approximately 58 km long on the northern side, 45 km long on the southern side and 11–15 km wide. On the southern side of the fjord there is a fjord arm Palanderbukta, which stretches south-east from Wahlenbergfjorden. Nordaustlandet is mostly covered by ice caps and glaciers and there are many calving glaciers coming into Wahlenbergfjorden especially on the northern side of the fjord.

In 2006 the position of the measuring camp was 79°44'N, 20°40'E and in 2007 79°39'N, 19°43'E. The positions are marked in the map (Figure 4.2). The ice conditions in Wahlenbergfjorden were different between the two years, and in 2006 the camp was further inside the fjord than in 2007. In 2006 the measurements lasted from May 9th to May 13th and in 2007 from April 18th to April 22nd.

4.2 Turbulence instrumentation

Sonic anemometers were used for fast response turbulence measurements. They provided measurements of three wind components and of sonic temperature. Sonic anemometers measure the instantaneous velocity components and air temperature using the transit times of acoustic signals transmitted along a fixed path and are the main instruments for direct measurement of turbulent fluxes of momentum and sensible heat.

A Sonic Anemometer/ Thermometer model SATI/3(K), manufactured by

Figure 4.1: *Map of the Svalbard archipelago (Norsk Polarinstitutt). Wahlenbergfjorden area is marked with a rectangle.*

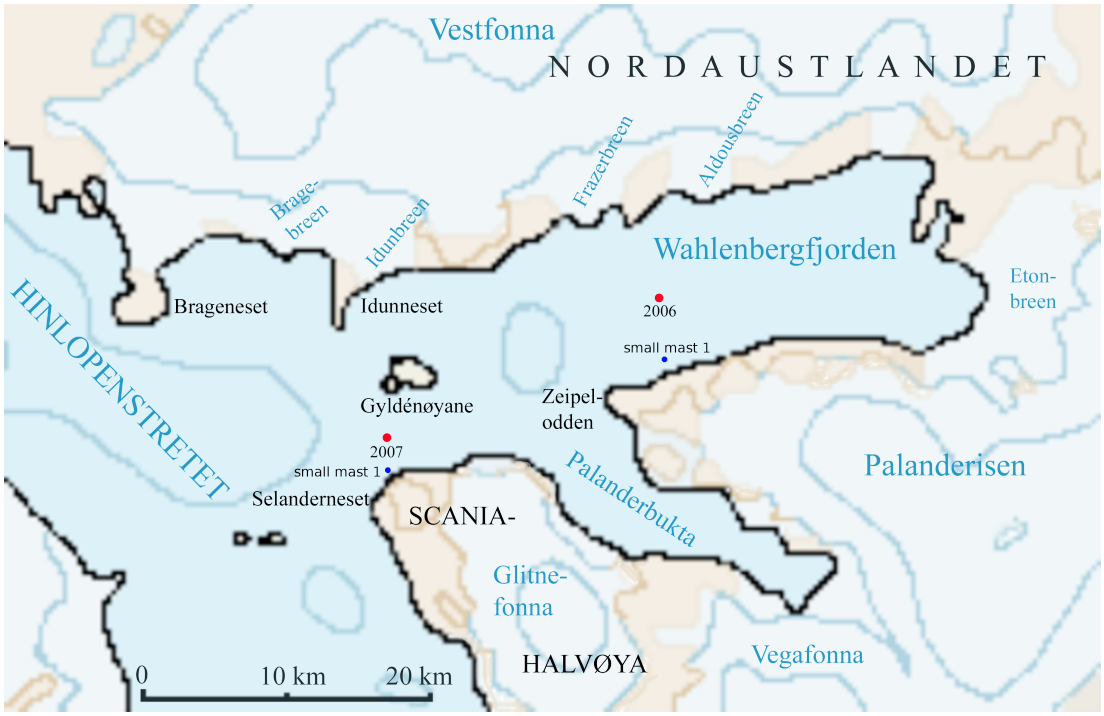

Figure 4.2: *Wahlenbergfjorden. The locations of the measuring camps in 2006 and 2007 are marked with red dots and the approximate locations of the small weather masts close to the shore are marked with blue dots.*

Applied Technologies, Inc., was used in 2006. The "K"-style probe assembly is ideal for atmospheric boundary layer studies, and it is designed to minimize probe-induced flow distortion. The three axes are separated, which imposes a minimum limit on the height at which the instrument can be operated with reliability. As suggested by Kaimal and Finnigan (1994), this probe is not suitable for use below 4 m where the vertical gradients of wind speed are typically the largest and the eddy scales of interest are too small to be resolved accurately. The instrument was mounted at 6.1 meters height, well above the recommended minimum height. The measurement frequency was 10 Hz.

In 2007 the instrument used was CSAT3 three-dimensional sonic anemometer, manufactured by Campbell Scientific. The errors caused by wind blowing normal to the sonic path are corrected by the instrument before the wind speed is transformed into orthogonal coordinates (Campbell Scientific, 1998). It is therefore unnecessary to apply the speed of sound correction that will be described in section 5.1.3. The measurement frequency was 20 Hz and the instrument was mounted at 2.7 meters height. In addition to the sonic anemometer, the measurement system included a LI-7500 open path infrared CO_2 and H_2O gas analyser, which measured carbon dioxide and water vapor concentrations with 20 Hz resolution.

All data treatment was done with Matlab. The obtained data was averaged over 30-minute periods. Variances and covariances were calculated and used for flux calculations.

4.3 Profile instrumentation

Profile instrumentation included one big weather mast and two smaller masts, one of which was placed close to the boat (referred to as the small mast 2) and the other one a few kilometers away from the boat, close to the shore on the southern side of the fjord (referred to as the small mast 1). The big weather mast had instruments on three levels, while the smaller ones measured at two levels. The sensors used were from Aanderaa instruments and measured wind speed (WS), wind gust (WG), wind direction (WD), temperature (AT), relative humidity (RH) and atmospheric pressure (AP) at one minute intervals. The setup of the masts is given in Figures 4.3 and 4.4.

The data treatment was done with Matlab. Spike detection was based on visual inspection of the data. Any unrealistic values were removed from the data and marked as missing values. After that, the data was averaged over 30-minute

periods. In order to avoid flow distortion, data collected during wind directions when the mast was downwind of the ship were not used.

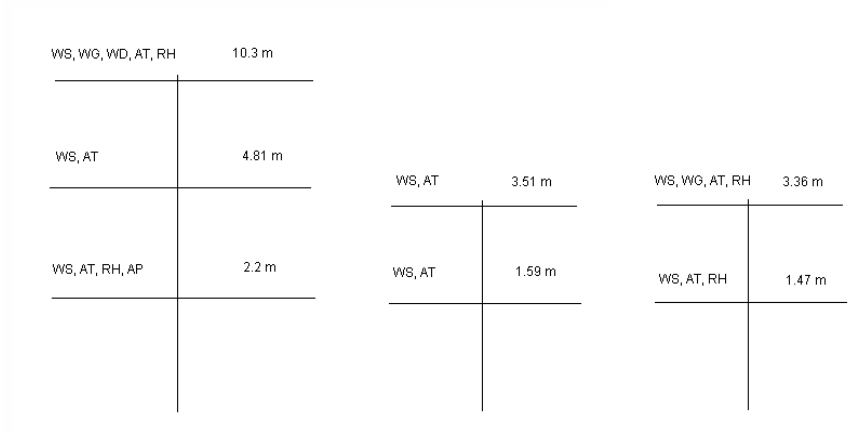

Figure 4.3: *Setup of the weather masts in 2006 with the big mast on the left, small mast 1 in the middle and small mast 2 on the right.*

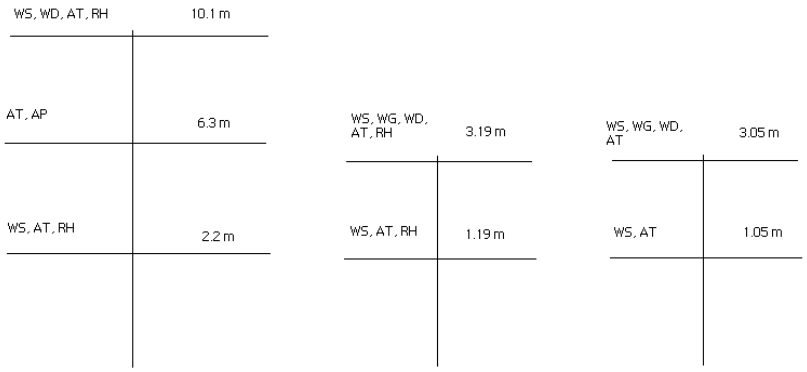

Figure 4.4: *Setup of the weather masts in 2007 with the big mast on the left, small mast 1 in the middle and small mast 2 on the right.*

5 Data and methods

5.1 Processing of the sonic anemometer data

5.1.1 Quality control

Data spikes can be caused by random electronic spikes in the monitoring or recording systems. Electronic spikes can be considered to have a maximum width of three consecutive points in the time series and amplitude of several standard deviations away from the mean (Vickers and Mahrt, 1997). In this study, any datapoint that was more than 3.5 standard deviations from the five minutes mean value was considered a spike. However, if four or more consecutive points were detected they were not considered spikes. Values which were detected as spikes were marked as missing values and excluded from later calculations.

Some of the main problems when using sonic anemometers are related to flow distortion. Flow distortion refers to the influences caused by the sensor arrangement of the anemometer itself, other sensors or supporting structures (Foken and Wichura, 1996). A correction cannot be performed in a simple way, but the problem can be avoided by pointing the anemometer to mean wind direction. This was not done in Wahlenbergfjorden, so the measurements contained data collected during unfavorable wind directions when the sonic anemometer was downwind of the mast or the ship. For the Wahlenbergfjorden measurements, problems caused by possible flow distortion were solved by discarding the data collected during unfavorable wind directions when flow distortion may have occurred.

5.1.2 Tilt correction

Coordinate tilt can occur in several ways. The most obvious one is a physical tilt of the instrument relative to the correct coordinate frame. A possible tilt of

the sonic anemometer was corrected by rotating the instrument coordinates to natural wind coordination. This can be done by applying a series of two rotations at the end of each 30 minutes turbulent averaging period after which the x-axis is aligned with the mean wind vector (Wilczak et al., 2001). A third sonic rotation is applied with the requirement $\overline{v'w'} = 0$. A positive covariance $\overline{u'w'}$ after rotation usually indicates problems with the sonic anemometer (Lee et al., 2004). Therefore datapoints with positive covariance $\overline{u'w'}$ were removed from the data and marked as missing values.

Let subscript 1 denote velocity components and coordinate axes in the instrument coordinate. To force the mean lateral and vertical velocities to zero, a rotation through an angle η around the z_1-axis and an angle θ around the y_1-axis is applied. The instant velocity components after the rotation, denoted with subscript 2, are (Lee et al., 2004)

$$u_2 = u_1(CT)(CE) + v_1(CT)(SE) + w_1(ST) \tag{5.1}$$

$$v_2 = v_1(CE) - u_1(SE) \tag{5.2}$$

$$w_2 = w_1(CT) - u_1(ST)(CE) - v_1(ST)(SE) \tag{5.3}$$

where

$$(CE) = \cos\eta = \overline{u_1}/(\overline{u_1}^2 + \overline{v_1}^2)^{1/2} \tag{5.4}$$

$$(SE) = \sin\eta = \overline{v_1}/(\overline{u_1}^2 + \overline{v_1}^2)^{1/2} \tag{5.5}$$

$$(CT) = \cos\theta = (\overline{u_1}^2 + \overline{v_1}^2)^{1/2}/(\overline{u_1}^2 + \overline{v_1}^2 + \overline{w_1})^{1/2} \tag{5.6}$$

$$(ST) = \sin\theta = \overline{w_1}/(\overline{u_1}^2 + \overline{v_1}^2 + \overline{w_1})^{1/2} \tag{5.7}$$

To force $\overline{u'w'}$ to zero, the intermediate z_2-y_2 plane must be rotated through an angle β. After this third rotation, we obtain (Lee et al., 2004)

$$u = u_2 \tag{5.8}$$

$$v = v_2(CB) + w_2(SB) \tag{5.9}$$

$$w = w_2(CB) - v_2(SB) \tag{5.10}$$

where

$$CB = \cos\beta \tag{5.11}$$

$$SB = \sin\beta \tag{5.12}$$

and

$$\beta = \frac{1}{2}\arctan\left[\frac{2\overline{v_2'w_2'}}{(\overline{v_2'^2} - \overline{w_2'^2})}\right] \tag{5.13}$$

5.1.3 Cross-wind correction

The strong dependence of speed of sound on temperature forms the basis for measuring temperature with a sonic anemometer. However, the temperature measurements are affected by the wind speed and must therefore be corrected for cross-flow contamination (Kaimal and Gaynor, 1991; Liu et al., 2001). The cross-wind contamination is caused by signal deflection of the sound path in the instrument, created by the perpendicular wind component. The contamination is significant in neutral and stable stratifications when temperature fluctuations tend to vanish or become very small. For virtual kinematic heat flux the correction can be calculated from (Kaimal and Gaynor, 1991)

$$\overline{w'T'_s} \approx \overline{w'T'_s(uncor)} + \frac{2U\overline{u'w'}}{403} \tag{5.14}$$

Because $u'w'$ is negative near the ground, the error term will always be positive. After this correction, fluctuations in sonic temperature should closely approximate fluctuations in the virtual temperature of air (Kaimal and Gaynor, 1991).

5.1.4 Moisture correction

The sonic temperature T_s, measured by the sonic anemometer, is not exactly the actual virtual temperature T_v. However, the error in assuming $T_s \approx T_v$ is on the order of 0.01 K, which is within the bounds of the measurement uncertainties (e.g. Kaimal and Gaynor, 1991). Therefore, T_s can be used instead of T_v. The difference between virtual temperature and actual temperature is frequently less than 2 K, but the virtual heat flux may differ significantly from the actual one (Arya, 2001). Therefore a correction should be applied. For the measurements in 2007, the real temperature was calculated using the fast-response measurements of water vapour content. The obtained real temperature was then used in covariance calculations. In 2006 these fast-response measurements of water vapour content were not done, so the correction was made directly to the sensible heat flux by using the simultaneously measured temperature and humidity profiles. To a good approximation the following relationship can be used to derive the actual sensible heat flux (Lumley and Panofsky, 1964):

$$\overline{w'T'} = \frac{\overline{w'T'_v}}{1 + \frac{0.07}{\beta}} \tag{5.15}$$

where β is the Bowen ratio. The Bowen ratio can be calculated from the gradient measurements of potential temperature and humidity, assuming that the exchange coefficients for heat and humidity are equal:

$$\beta = \frac{c_p \frac{\partial \theta}{\partial z}}{\lambda \frac{\partial q}{\partial z}} \tag{5.16}$$

where q is the specific humidity and λ the latent heat of evaporation.

5.2 Methods for determining turbulent fluxes

5.2.1 The eddy correlation method

The eddy correlation method is the most direct and reliable way to determine turbulent fluxes of heat, momentum and moisture in the near-surface atmospheric layer. The advantage of using this method is that turbulent exchanges are measured directly and not too many assumptions about the surface and the atmosphere are required. It is therefore often used as a reference method in estimating other methods. It is a simple method of determining fluxes, but requires the use of fast-response sensors, such as sonic anemometers, with a sampling rate of 10-20 Hz. It is also sensitive to flow distortion. Once the covariances $\overline{u'w'}$ and $\overline{w'\theta'}$ have been calculated from the sonic anemometer measurements, the turbulent fluxes of momentum (τ) and sensible heat (H) can be calculated directly as

$$\tau = -\rho \overline{u'w'} \tag{5.17}$$

$$H = \rho c_p \overline{w'\theta'} \tag{5.18}$$

where ρ is the density of air (assumed constant $\rho = 1.225 kgm^{-3}$) and c_p the specific heat of air for constant pressure ($c_p = 1005 Jkg^{-1}K^{-1}$).

5.2.2 Gradient method

The gradient method is used to determine fluxes from mean vertical gradients of velocity, temperature or moisture between two arbitrary heights in the surface layer. The turbulent fluxes of momentum τ and heat H in gradient forms can be expressed as

$$\tau = \rho \left[\frac{k\Delta U}{\phi_m ln(z_2/z_1)} \right]^2 \tag{5.19}$$

$$H = -\rho c_p \left[\frac{k^2 \Delta U \Delta \theta}{\phi_m \phi_h (ln \frac{z_2}{z_1})^2} \right] \tag{5.20}$$

The fluxes are sensitive to accuracy of the wind speed and temperature difference between the two observation levels and the ratio between the levels. The vertical gradients can be calculated using finite-difference approximations. Logarithmic approximation is normally used, since the mean profiles are usually logarithmic with height. The gradients are then calculated for the geometric mean height $z_m = (z_2 z_1)^{1/2}$, where z_1 is the lower and z_2 the upper measurement level. However, in very stable conditions the linear approximation might be superior, because mean velocity and temperature profiles are more nearly linear, especially in the upper part of the surface layer (Arya, 2001). The ratio of z_1 and z_2 should not be too large, when the finite-difference approximations may not be good enough, or too small, when the differences between the two levels may not be well resolved. Good measurement heights are such that $z_2/z_1 = 2$ to 4 (Arya, 2001).

The similarity functions ϕ_m and ϕ_h can be calculated on the basis of the Richardson number. If the Richardson number exceeds the critical value of 0.2, the stability correction cannot be calculated from Equation 2.4.

Another option is to use an iterative method to calculate the fluxes. In doing so, the use of Richardson number is avoided since the stability corrections are determined by iteration. In this study, the iterative calculation method presented by Launiainen and Vihma (1990) was used for calculating turbulent surface fluxes under stratified conditions. In this process neutral stability is assumed during the first calculation loop and first guess for fluxes is calculated for a neutral case. After that, new corrected universal functions are calculated and used in the next calculation loop. Iteration is performed until convergence is achieved. Convergency depends on the stratification in the surface layer. For unstable conditions the iteration will converge, but for stable cases, there is a limit for convergency. Also the universal function formulae used affect the ability of convergency (Launiainen and Vihma, 1990).

5.3 Calculation of the aerodynamic roughness length

Frictional drag causes the wind speed to become zero close to the surface. The rougher the underlying surface, the more the wind is affected by surface drag. The aerodynamic roughness length z_0 is defined as the height where the wind speed goes to zero and it is a measure of the surface roughness. It is not equal to the height of the individual roughness elements, but is determined for a particular surface. Once determined, it is usually assumed not to change with stability, wind speed or stress, as long as the surface roughness itself does not change.

The roughness length can be calculated by

$$z_0 = z/exp\left[\frac{kU}{u_*} + \psi_m\right] \tag{5.21}$$

where ψ_m represents the stratification correction to the logarithmic wind profile. The roughness length varies over many orders of magnitude for different surfaces. Usually the values for snow-covered sea ice are on the order of $10^{-3}m$ to $10^{-4}m$.

6 Results from Wahlenbergfjorden

In this chapter the results from the two measurement campaigns in 2006 and 2007 in Wahlenbergfjorden are presented. First, the general temperature and wind conditions along with stability conditions during the measurement periods are studied. Synoptic situation is investigated. Spatial variability and local effects are studied by comparing data from the weather masts at different locations. The turbulent fluxes of momentum and heat measured by a sonic anemometer are compared with fluxes derived from wind speed and air temperature profiles. Finally, the influence of stability on the non-dimensional gradients of wind speed and potential temperature is studied.

6.1 Meteorological conditions in 2006

The evolution of temperature, wind speed and wind direction measured by the sonic anemometer and the big weather mast instruments during the measurement campaign in May 2006 is presented in Figure 6.1. Unfortunately, the sonic anemometer data do not cover more than two days.

The temperature varies between -2°C and -7°C with the highest temperatures in the beginning of the measuring period. The temperature measured by the sonic anemometer is the sonic temperature. It is slightly higher than the temperatures measured with the weather mast sensors, which is expected as the sonic temperature is closer to the virtual temperature than the actual temperature. The wind speed has a spike on the 10th of April reaching about 12 ms^{-1}, otherwise the wind speed did not exceed 10 ms^{-1}. The sonic anemometer measured lower minimum wind speeds. The wind direction stays fairly constant and is mostly between 240 and 360 degrees, changing from along-fjord to cross-fjord winds during the measurement period. The wind directions measured with the sonic anemometer and the weather mast wind direction sensor correlate well.

The stability parameter calculations from the measurements in 2006 are

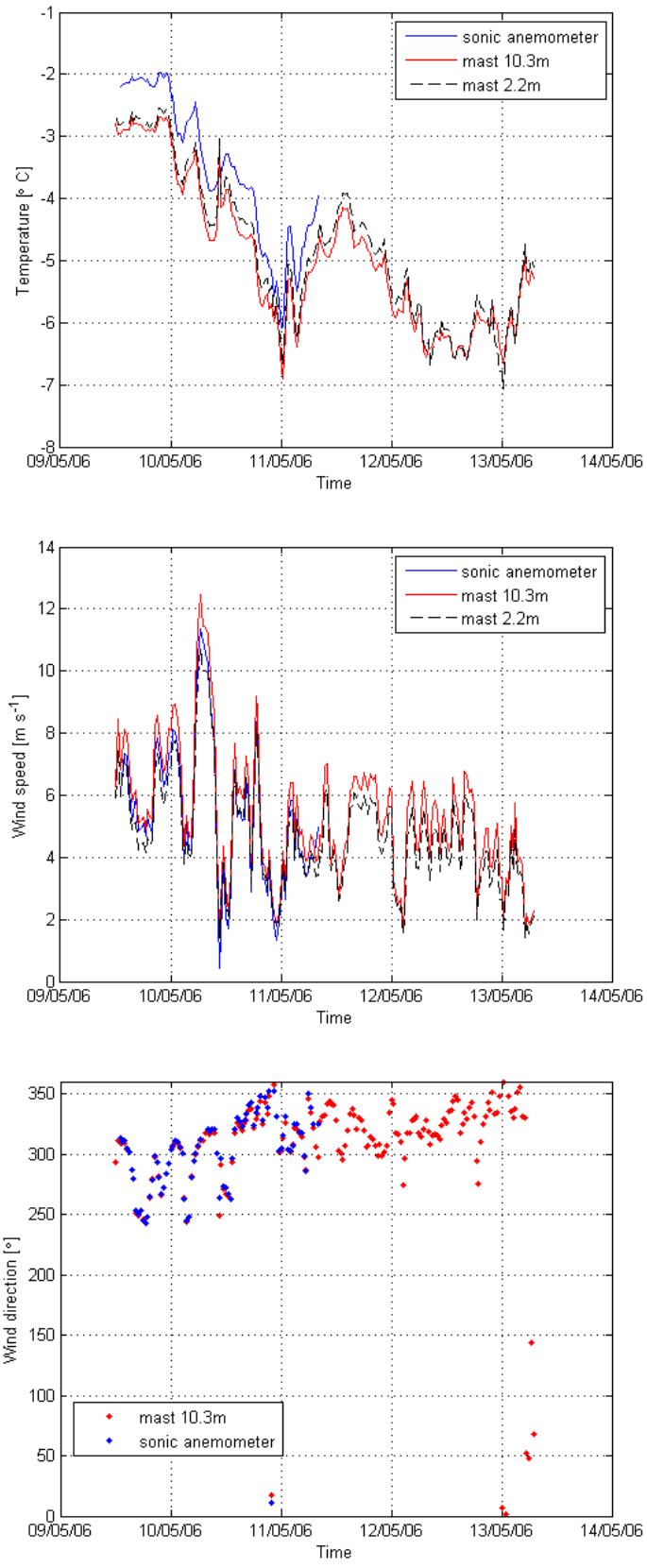

Figure 6.1: *Time series of temperature, wind speed and wind direction measured in Wahlenbergfjorden in May 2006.*

presented in Figure 6.2. The stability parameter was calculated from the sonic anemometer measurements using the Obukhov length (Equation 2.2) and from the profile measurements on the basis of the Richardson number using Equations 2.3 and 2.4. For $Ri > 0.2$, the stability parameter was not calculated. Positive stability parameter indicates a stably stratified surface layer, whereas negative values are observed when the surface layer is unstable. The sonic anemometer shows stable stratification from the beginning of the time series until the morning of 10th of May, but weather mast measurements suggest mostly unstable stratification for that time. After that, both sonic anemometer and weather mast indicate unstable stratification.

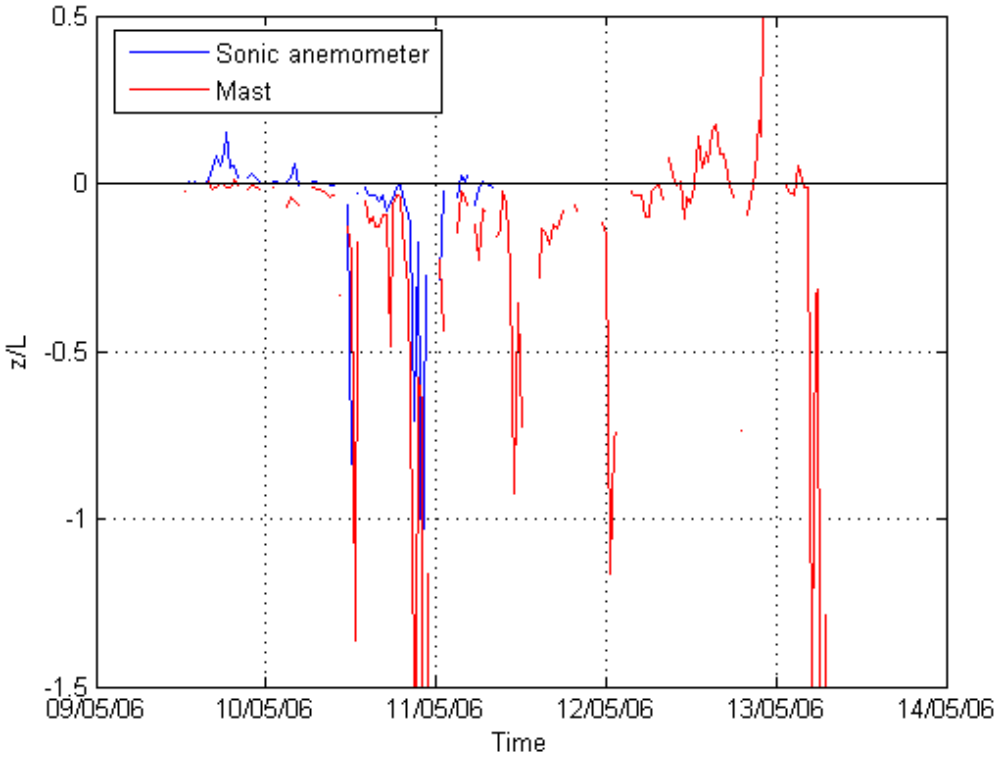

Figure 6.2: *Time series of the stability parameter z/L in 2006.*

6.2 Meteorological conditions in 2007

Figure 6.3 shows the temperature, wind speed and wind direction measured during the field campaign in April 2007. The temperature measured by the sonic anemometer has been converted to real temperature. The upper and lower

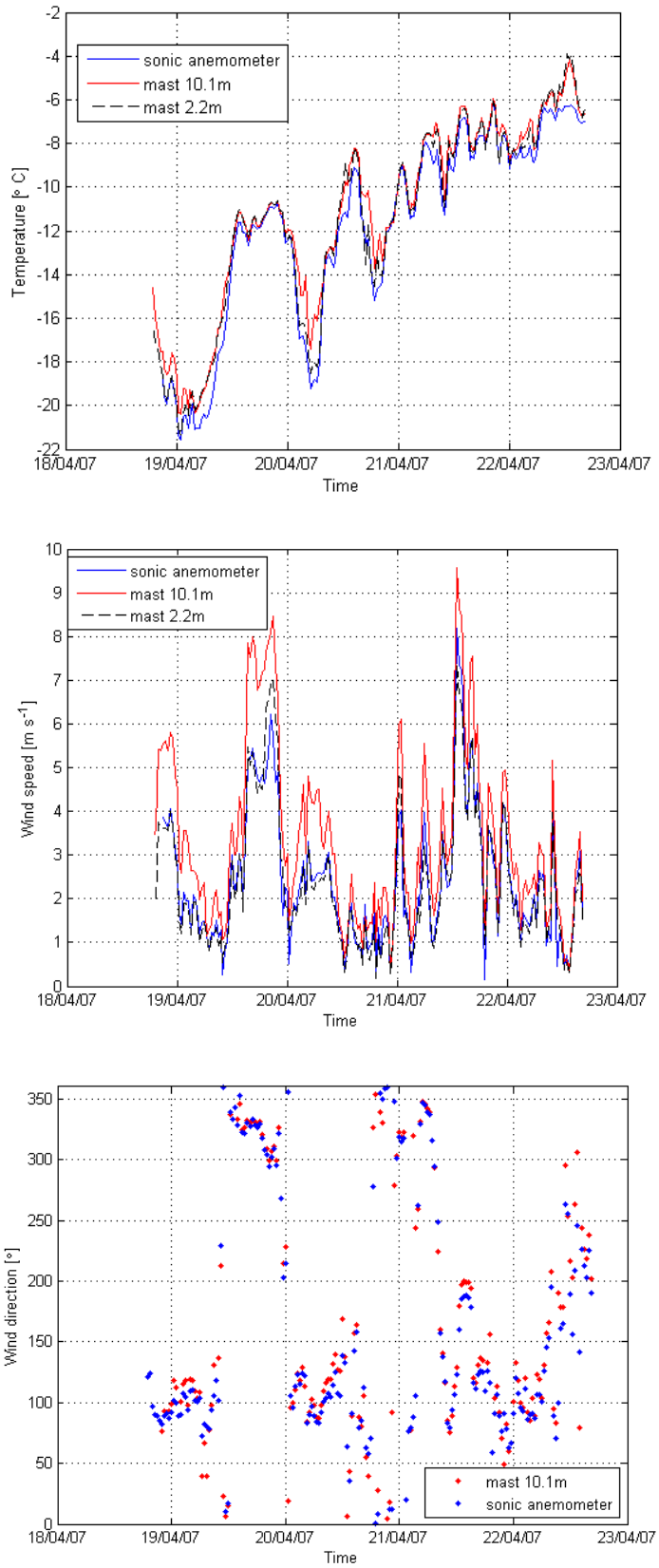

Figure 6.3: *Time series of temperature, wind speed and wind direction measured in Wahlenbergfjorden in April 2007.*

temperature from the weather mast closely follow each other, the lower being slightly colder most of the time. Largest temperature variations are observed during the 19th and 20th of April, when the temperature increased by about 10 degrees. The wind speed has two of peaks, on the evening of 19th of April, when the increase in wind speed is accompanied by a rapid change in wind direction, and on the 21st of April after midday. Both of these peaks occurred during cross-fjord winds, the first one with wind coming from north-west and the second one during a short period of southerly winds. The wind direction was mainly around 100 degrees, which implies winds along the fjord axis out of the fjord.

Figure 6.4 shows the stability parameter obtained from the sonic anemometer measurements and calculated from the profile measurements. The stability parameter fluctuates between positive and negative values and in most cases the stable or unstable periods lasted less than 12 hours. The time series shows many spikes both in the sonic anemometer and weather mast measurements, some of which occur at the same time. 76 % of the time the sign is the same.

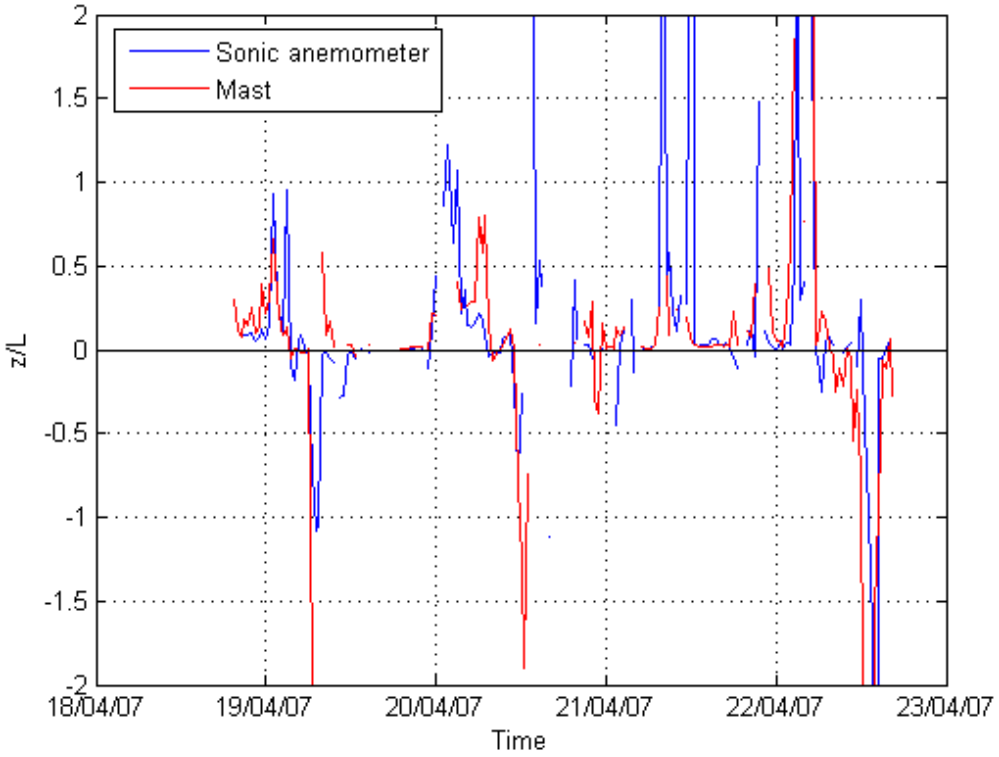

Figure 6.4: *Time series of the stability parameter z/L in 2007.*

6.3 Effects of the synoptic scale variations

Due to the shortness of the time series, the presented results mainly reflect the large-scale weather conditions during the measurement periods. Therefore, it is useful to link the measurements to the synoptic situations to distinguish between the large-scale effects and local effects.

Observations for the area in question are sparse or none. Therefore, European Centre for Medium-Range Weather Forecasts (ECMWF) operational analysis fields are used for the interpretation of synoptic situations. Figures 6.5 and 6.6 present the mean sea level pressure and temperature at 850 hPa during the measurement period in 2006. Figures 6.7 and 6.8 are the same for 2007.

Based on the pressure maps, the prevailing geostrophic wind direction during the measurements in 2006 was from the north-west, turning more north at the end of the measurement period. At the same time, the pressure gradient weakened. Thus, measured wind direction followed the large-scale flow direction, and the weaker pressure gradient showed as weaker winds. Temperature gradient at 850 hPa was weak and determining large-scale heat advection is hard. The observed unstable stratification indicates that there might have been cold advection. The strong pressure gradient also favoured the existence of unstable or neutral stratification. Some warm advection probably occurred at the end of the measurement period. This can also be seen in the stratification, which changes from unstable to stable. The weaker winds resulting from the weakened pressure gradient also allowed stable boundary layer to develop.

In 2007, the pressure gradient was weaker. There is a weak, filling low pressure centre over Svalbard area, first located south-east of Nordaustlandet, then moving to western side of Svalbard. We can assume a relatively weak flow with a change in direction from north-east to south-east. Temperature gradient was relatively strong in the beginning of the measurement period, weakening towards the end. Due to weak pressure gradient, heat advection was probably quite weak. Some warm advection is likely to have occurred. Weak flow combined with warm advection explains why several periods of stable stratification occurred in 2007. This situation is also favourable for the occurrence of mesoscale phenomena such as katabatic winds or channelling of winds.

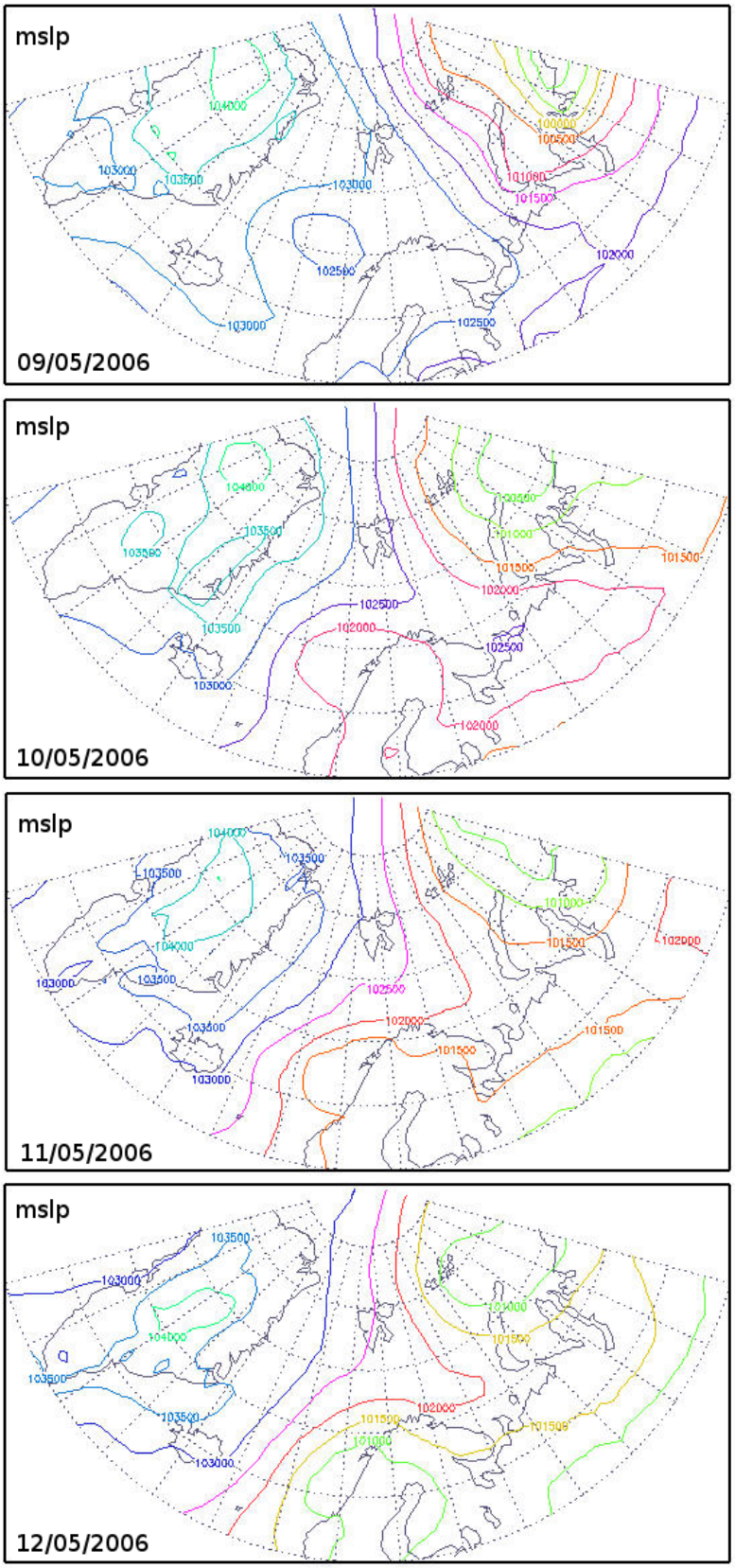

Figure 6.5: *Mean sea level pressure ECMWF analysis fields for the measurement period in May 2006. All maps are for 12 UTC.*

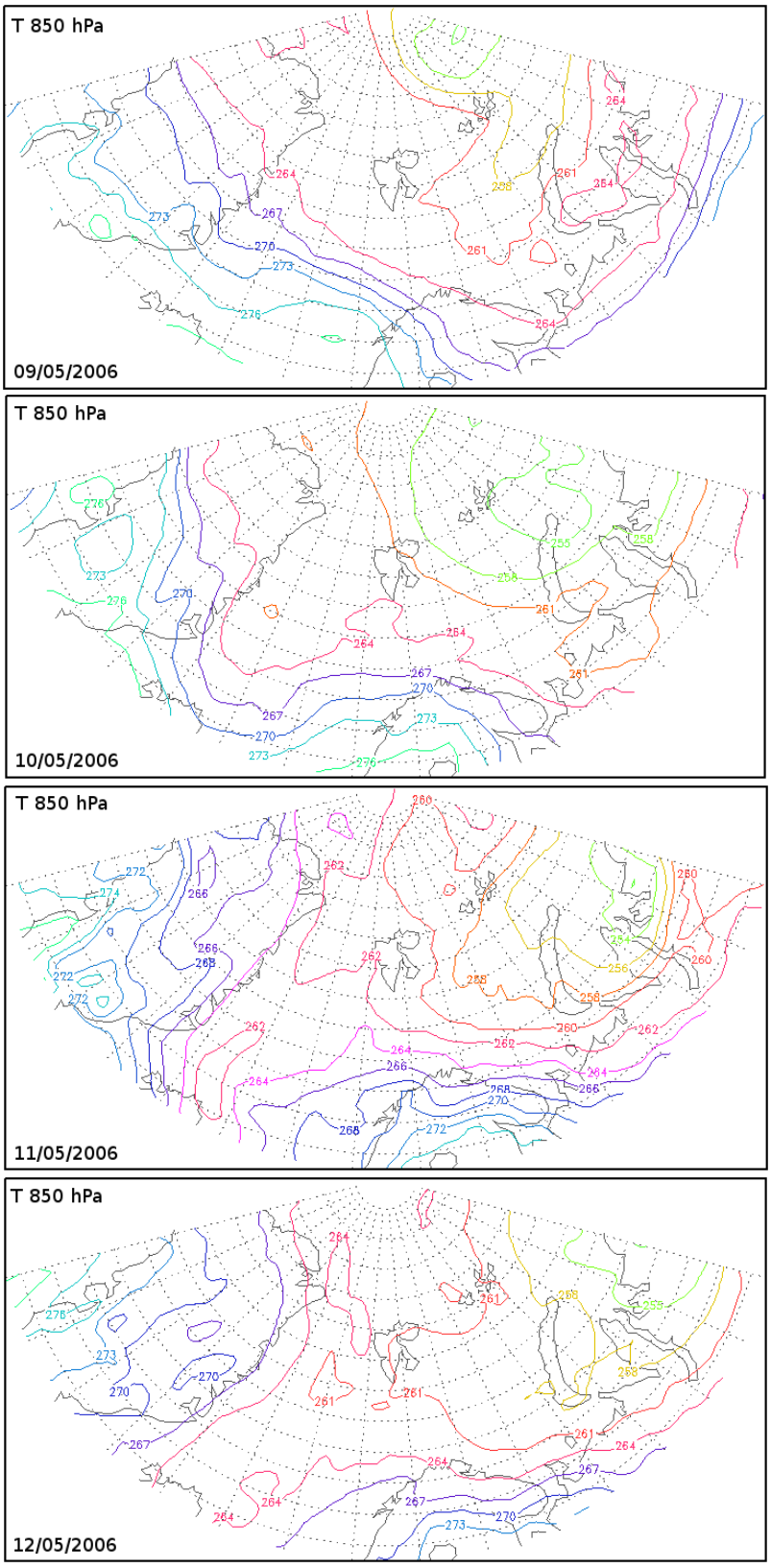

Figure 6.6: *850 hPa temperature ECMWF analysis fields for the measurement period in May 2006. All maps are for 12 UTC.*

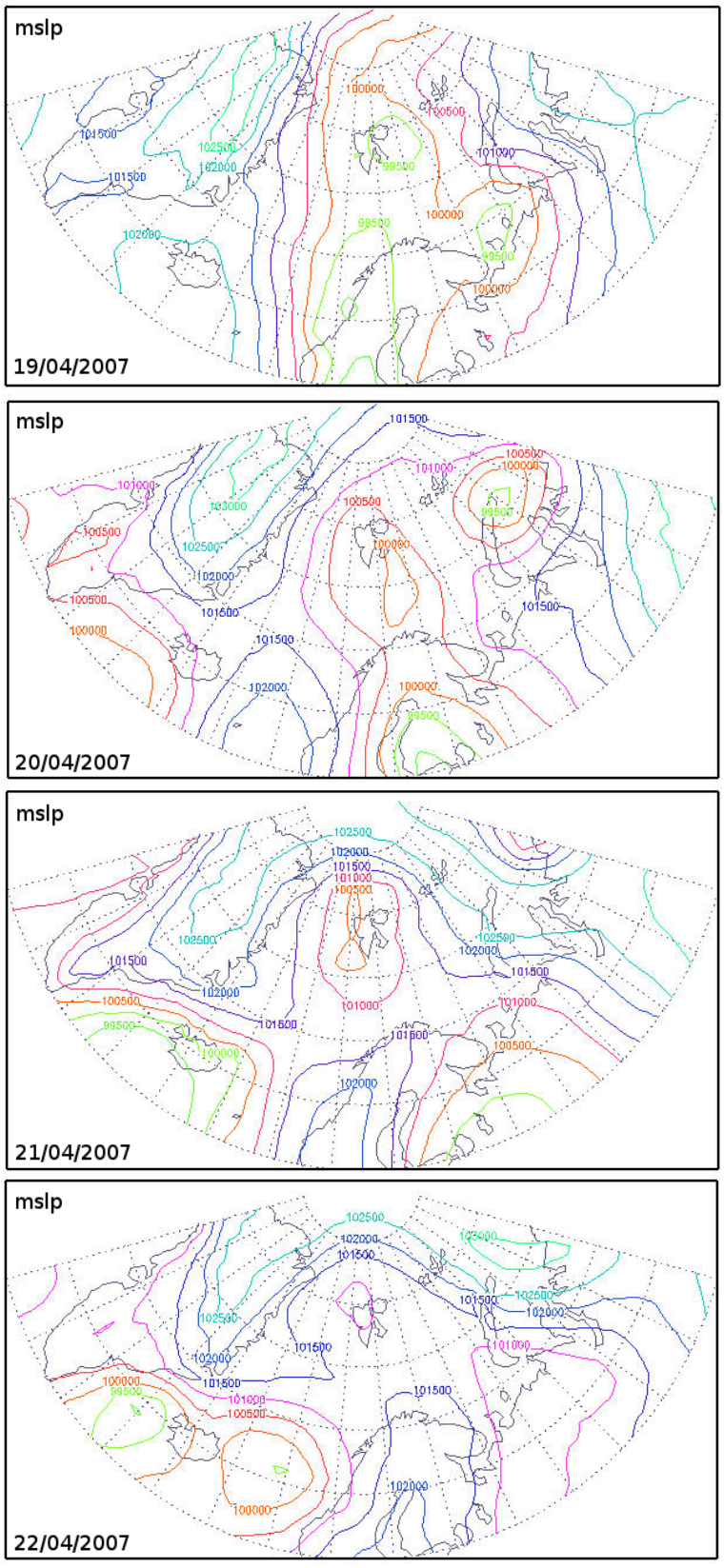

Figure 6.7: *Mean sea level pressure ECMWF analysis fields for the measurement period in April 2007. All maps are for 12 UTC.*

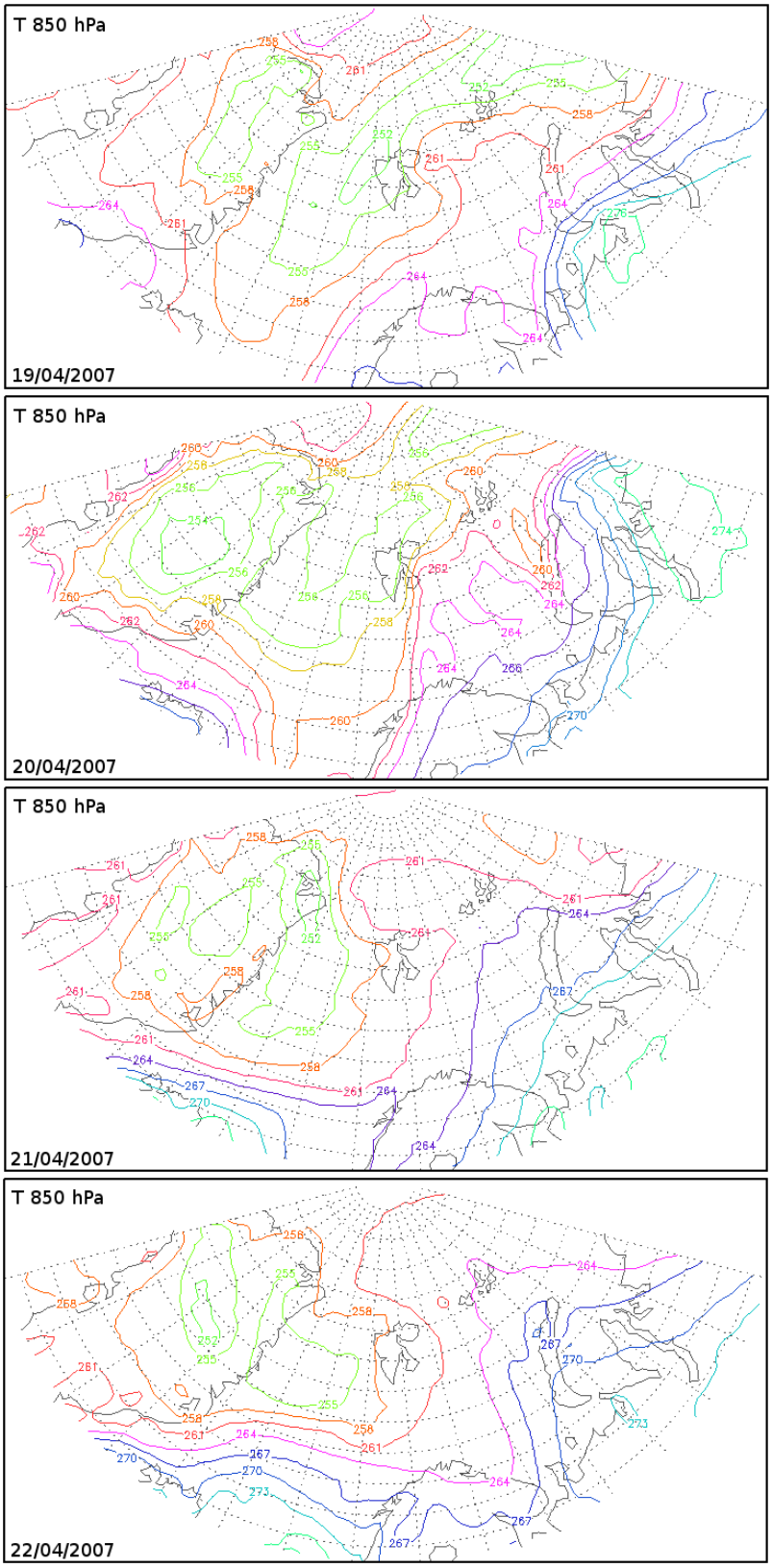

Figure 6.8: *850 hPa temperature ECMWF analysis fields for the measurement period in April 2007. All maps are for 12 UTC.*

6.4 Spatial variability

The boundary layer over land-fast fjord ice has different features than boundary layer over pack ice in the Arctic ocean, since also topography plays a role. The topographic effects may include channelling, drainage flows and mountain waves. The flow is more easily disturbed by local effects in a smaller valley than a large one. Wahlenbergfjorden is a rather large fjord and it is wide enough to allow cross-fjord winds, but also channelling effects take place. The wind in the middle of the valley is more likely to follow the large scale flow than the wind on the sides, which is more prone to effects of katabatic flows. Therefore it is very useful to investigate the results from weather masts in different locations. The local influences are different between the stations and also vary with wind direction at each station. Mountainous topography affects the flow field in many ways. Therefore, the typical wind conditions for a particular site are hard to determine without long-term measurements, which were not available for Wahlenbergfjorden.

The weather masts were located away from each other. Both in 2006 and 2007, the distance between the big weather mast and the small mast 2 was approximately 200 meters, while the small mast 1 was located a few kilometres away, closer to shore. It is therefore possible to make comparisons between the data from the weather masts in different locations to see if there is variability caused by topography or surface inhomogeneities. The following section presents the results from year 2007. In 2006, the small weather masts did not have wind direction sensors, so similar comparisons against wind direction could not be done for that year. In 2007, there was a clear bias in the wind direction measurements from the small mast 2, possibly connected to calibration. The error has been corrected for small mast 2 wind directions that were measured at the same time with big mast wind directions 0°–220°. This was done by making a linear correction to the small mast wind direction data so that it matched the big mast wind direction data. The rest of the small mast 2 wind directions have not been corrected since the datapoints were too scattered. Thus, part of the wind direction results from small mast 2 may be unreliable.

Wind roses for the three weather masts in 2007 are presented in Figure 6.9. Figure 6.9(c) presents the corrected wind direction from small mast 2. Differences between the masts can be found. The big weather mast shows one clear main wind direction out of the fjord. The small mast close to the shore shows both winds along the fjord and cross-fjord winds from the south. The small mast 2 and the

big weather mast were located relatively close to each other and thus give similar results. The small mast 2 was located only 60 meters away from the boat and flow distortion caused by the ship may have disturbed some of the observations.

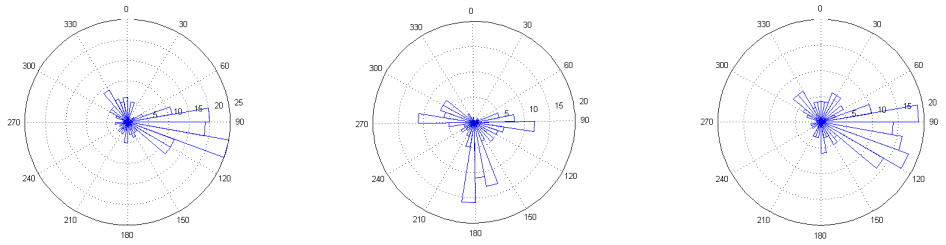

(a) big mast (b) small mast 1 (c) small mast 2

Figure 6.9: *Wind roses from three masts in 2007. Small mast 1 was close to shore and small mast 2 close to the boat.*

Figure 6.10 shows the scatter plots of wind speed and roughness length z_0 (Equation 5.21) against the wind direction. The wind speed and the wind direction from the big weather mast in Figure 6.10(a) are measured at the uppermost level, which explains the higher wind speeds compared to the sonic anemometer, which was placed several meters lower. The wind speeds in Figures 6.10(b) and (c) are also measured at the upper level. The roughness lengths are plotted in a semi-log scale since the values range over several magnitudes.

Both the big weather mast sensors and the sonic anemometer measured maximum wind speeds from a cross-fjord direction around 180°-200°, but there are just a few observations of winds from this direction. The main direction with most observations is the along-fjord sector of 80°-130° with wind speeds varying mainly from 1 to 6 ms^{-1}.

The same scatter plots for the small weather mast located close to shore also show the same direction around 100° as can be seen in (a). There are some observations of high wind speeds over 8 ms^{-1} from this direction, but mainly the winds coming from this direction did not exceed the speed of 4 ms^{-1}. The direction around 150°–180° also shows some higher wind speeds. The largest roughness lengths are observed for this direction although there is a lot of scatter in the roughness length values. Only the sector 250°–300° shows quite a small variation of z_0. This station did not record northerly winds unlike the two other stations.

The small weather mast close to the boat measured lowest wind speeds of all

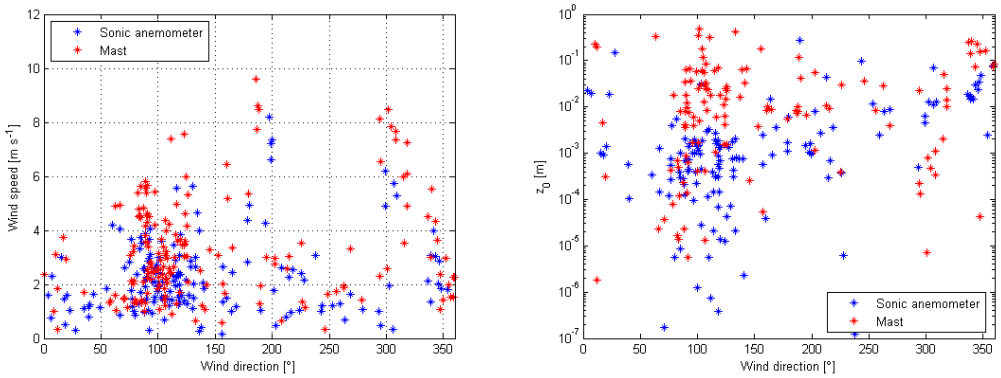

(a) Big mast (b) Big mast

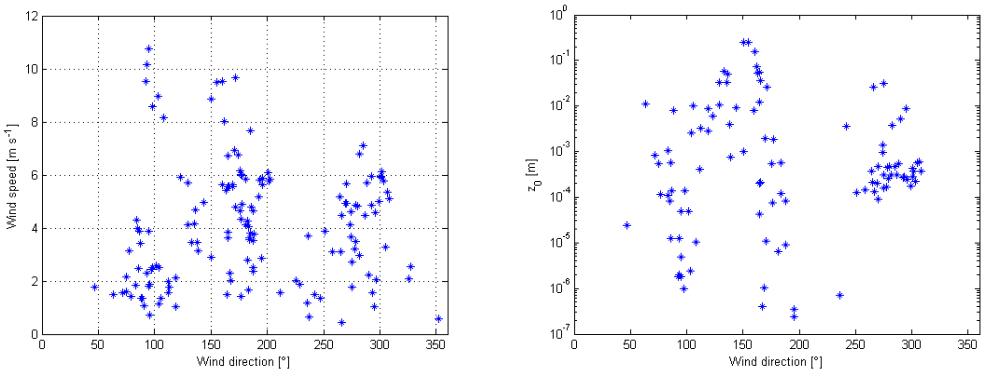

(c) Small mast 1 (d) Small mast 1

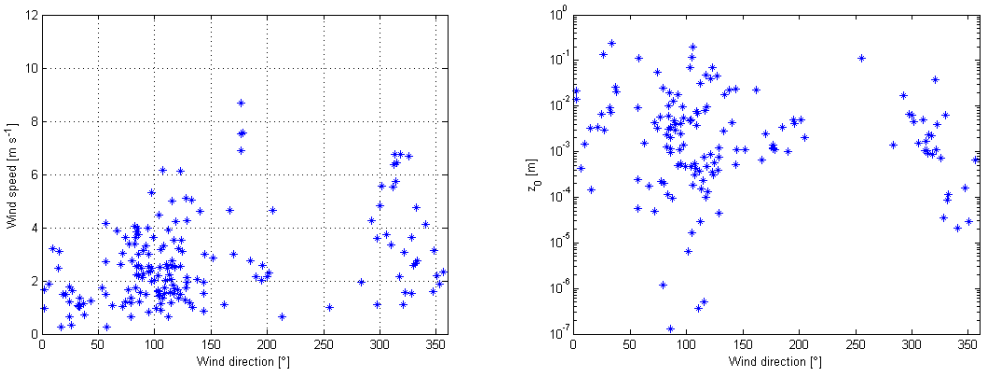

(e) Small mast 2 (f) Small mast 2

Figure 6.10: *Dependence of wind speed ((a), (c), (e)) and roughness length z_0 ((b), (d), (f)) on wind direction as measured by the three weather masts in 2007. Small mast 1 was close to shore and small mast 2 close to the boat.*

the masts. Otherwise the distribution of wind speeds looks similar to that of the big mast. Roughness length shows a lot of scatter for wind directions around 100°, for other directions the scatter is smaller.

The occurrence of the easterly winds along the fjord axis during the measurements in 2007 (see Figures 6.3, 6.9(a) and 6.9(c)) may imply channelling effects. Synoptic scale flow was relatively weak, which gave rise to channelling effects. However, more data during different synoptic flow conditions would be needed to distinguish prevailing main wind directions or channelling effects reliably. The channelling effect can also combine with drainage winds, resulting in higher wind speeds. There are glaciers also in the east, at the end of the fjord.

In 2006 the wind direction stayed fairly constant during the four days measuring period. The wind direction in 2006 was dominated by north-westerly wind direction due to relatively strong large-scale flow from that direction.

In 2007, the small mast 1 was placed on the southern shore of the fjord in front of a valley opening, which leads up to a glacier. This is a location which is likely to experience drainage flows from the glacier. This effect can clearly be seen in the wind rose, which shows a regular occurrence of southerly winds from the direction of the nearby glacier. To study the occurrence and effects of a possible drainage flow, time series of additional parameters were plotted (Figure 6.4). In the beginning of 20th of April the wind direction changes to southerly for a while. This change is accompanied by a drop in temperature and relative humidity. The change in temperature seems to follow the drop in relative humidity. These could be indications of a katabatic flow transporting colder and less humid air from the glacier. After midday on the 20th, the same changes are seen, only with a smaller drop in relative humidity. Around midday on the 21st of April the wind direction is southerly again and the relative humidity decreases, but noticeable changes in temperature do not occur. However, katabatic winds may also mix the stratified air, breaking up the inversion, and thus may not always produce a cooling effect. Southerly winds are again observed on 22nd of April around midday. The wind speed does not seem to be a good indicator of katabatic flows in this case.

The effects of the katabatic flow may extend quite far on flat land, especially in stably stratified conditions. However, southerly winds are almost nonexistent in the big weather mast measurements. The katabatic flow may not have been strong enough to extend this far. This conclusion is supported by the fact that the temperature in the big weather mast did not experience the same cooling that was observed by the small mast.

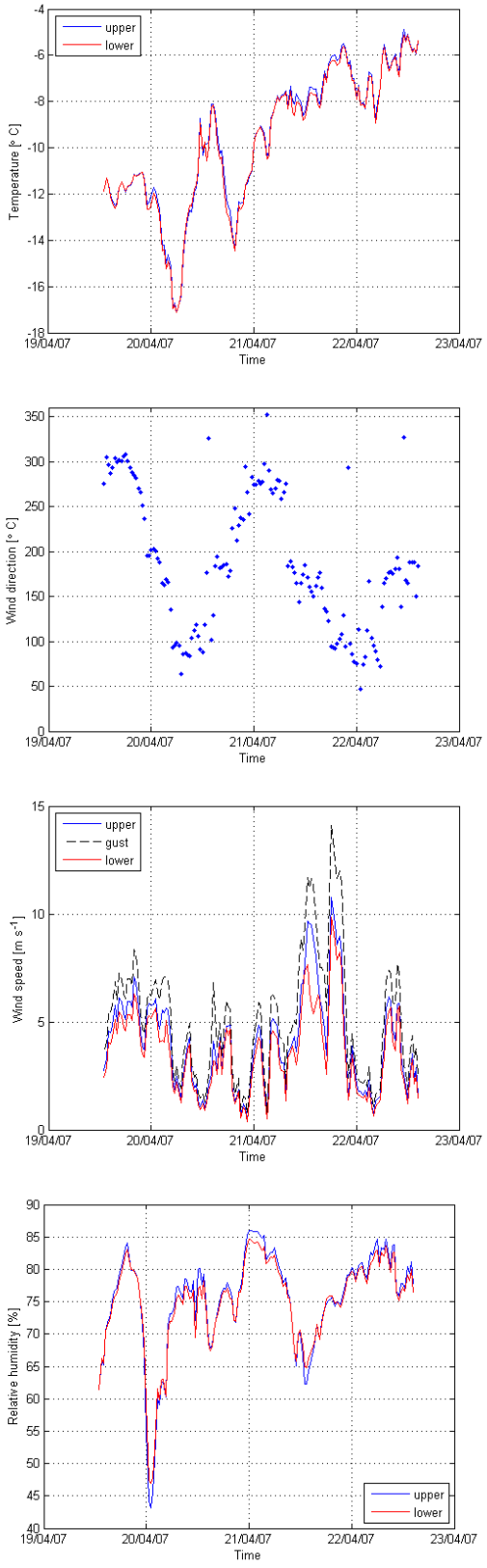

Figure 6.11: *Temperature, wind direction, wind speed and relative humidity from the small mast located close to shore in April 2007.*

Plots of the roughness parameter against wind direction reveal the effects of local and regional surface conditions. Reduced surface roughness was expected to be found for wind directions along the fjord axis. The roughness lengths in 2007 show quite a variation (see Figures 6.10 (b), (d) and (f)) but reduction for directions along fjord axis can be seen. Based on sonic anemometer measurements, the difference in roughness length for along-fjord directions and cross-fjord directions was found to be statistically significant at a 99.9 % confidence level. The mean value for along-fjord directions (60°–120° and 240°–300°) was $2.4 * 10^{-4}m$. For cross-fjord directions (150°–210° and 330°–30°) the mean value was found to be $5.4 * 10^{-3}m$. In 2007 there were pressure ridges located east and west of the measurement site. This probably resulted in bigger roughness lengths also for directions along fjord axis. Despite the large variation, most of the values are in the range of values expected for sea ice, which are on the order of $10^{-3}m$ to $10^{-4}m$.

Roughness length is traditionally used to describe a particular surface, and once determined, it is thought not to change with stability or wind speed. Thus, the roughness length at each station should only vary with wind direction due to different terrain types in different directions. However, in this study a weak connection between wind speed and roughness length was found (Figure 7.6), although the scatter is quite large. Positive correlation between the roughness length and wind speed was found to statistically significant at a 95 % confidence level. Moreover, the scatter of z_0 decreases with increasing wind speed. There are some indications that over snow-covered sea ice, the roughness length can indeed be a function of wind speed (Andreas et al., 2005). It is also possible that the roughness length changed during the measurement period due to surface changes caused by snowfall or snow drift, for example. Several cases of snowfall were observed during the measurement period, but exact times are not recorded. Snow drift may occur when wind speed exceeds 8 ms^{-1}. Such high wind speeds were measured only a couple of times. In contrast to the traditional assumption, there are indications that the roughness length can also be dependent on the stability (Zilitinkevich et al., 2008).

6.5 Turbulent surface fluxes

The turbulent fluxes of momentum and sensible heat were calculated with the eddy correlation method from the sonic anemometer measurements (Equations

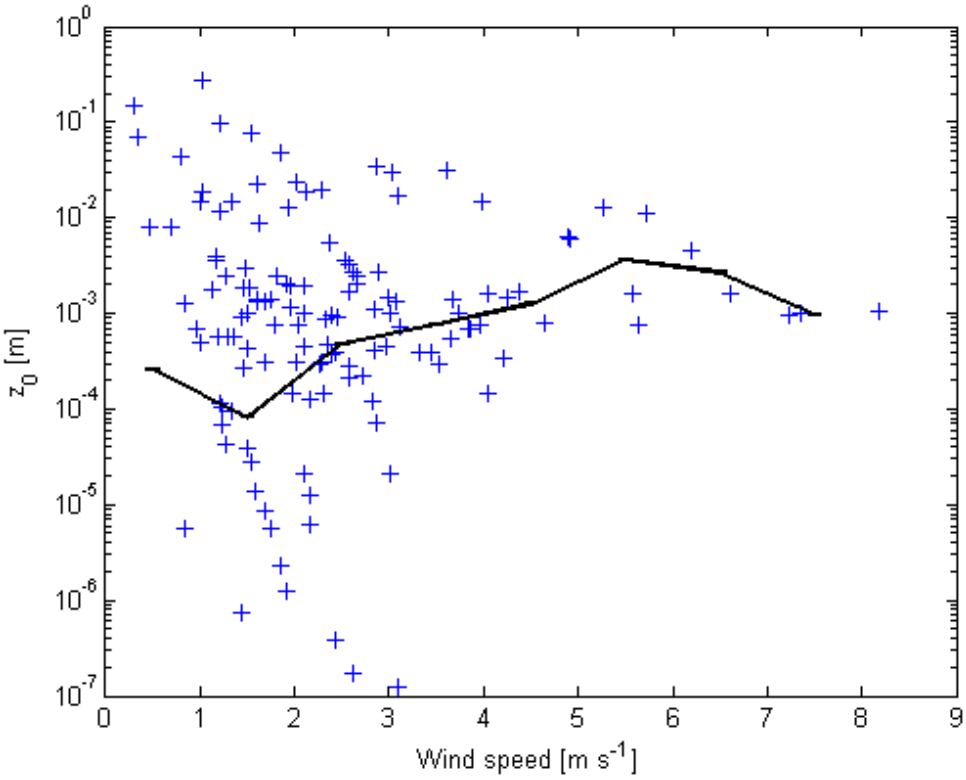

Figure 6.12: *Roughness length z_0 calculated from sonic anemometer measurements in 2007 plotted against wind speed. The solid line represents the z_0 values averaged in bins that are 1 ms^{-1} wide.*

5.17 and 5.18) and with the gradient method based on the profile measurements from the big weather mast, using an iterative algorithm. The eddy correlation method is the most direct way to determine fluxes and the results using this method can be regarded as the most reliable. Therefore it is used as a reference method and fluxes obtained from the gradient method are compared to the eddy correlation method. The fluxes are positive when directed away from the surface and negative when directed toward the surface.

The turbulent fluxes of momentum and sensible heat during the measurement campaign 2006 are presented in Figure 6.13. The gradient method calculations were made using three different combinations of the measurement levels.

The gradient method calculations of the momentum flux give very good estimates compared to the eddy correlation method. The peaks mostly match both in time and magnitude. The gradient method using different levels gives quite similar results.

Largest peaks are found at the beginning of the time series, on 9th and 10th

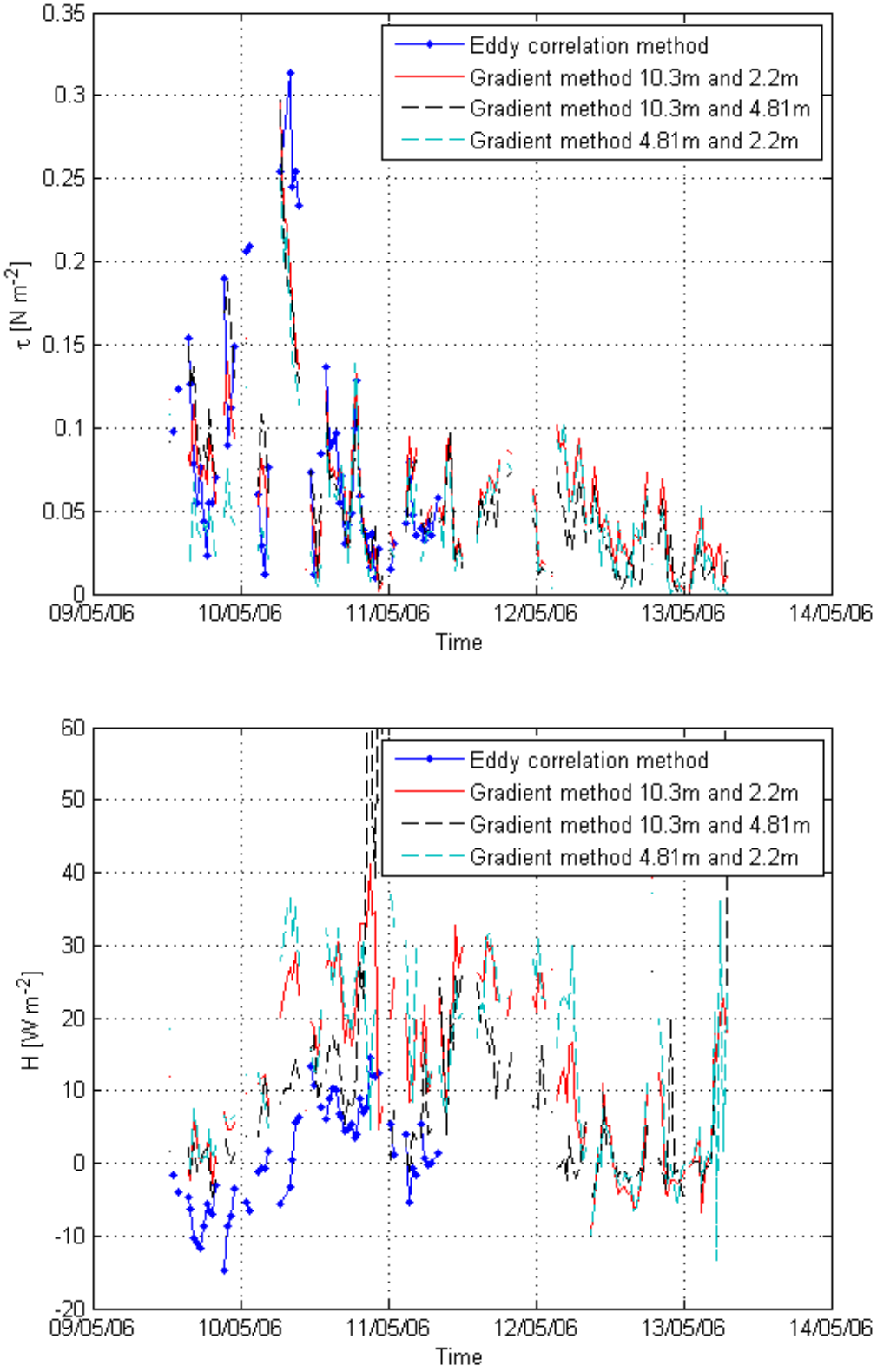

Figure 6.13: *Time series of the turbulent fluxes of momentum τ and sensible heat H measured in Wahlenbergfjorden in May 2006.*

of May, after that the flux stays small. A correlation between the momentum flux and wind speed (see Figure 6.1) can be seen, and the correlation coefficient was found to be 0.84 for sonic anemometer measurements. It seems that there is no diurnal cycle. This may be due to synoptic scale variations, which dominate over the diurnal cycle, but there are too few data to conclude that.

There is more variation between the profile measurements and the direct measurements of the heat flux. The sensible heat flux calculated from the weather mast measurements is mostly positive, indicating an upward heat flux. The results from the sonic anemometer are very different, showing a downward, small heat flux in the beginning of the time series. On the 10th of April the heat flux becomes mostly positive. The magnitude of the heat flux measured by the sonic is relatively small with values ranging from -15 Wm^{-2} to +15 Wm^{-2}. The gradient method using the two uppermost levels is most of the time closest to the eddy covariance measurements although the values are too large and, especially in the beginning of the time series, also of the wrong sign. The heat flux did not show a diurnal cycle either.

Figure 6.14 shows the turbulent fluxes of momentum τ and sensible heat H measured with the sonic anemometer and calculated from the profile measurements in 2007. The profile calculations from the big weather mast data were done using data only from the uppermost and lowermost levels, since wind speed observations were not available from the middle level.

The momentum flux calculated with the gradient method is larger than that from eddy covariance measurements almost throughout the time series. The gradient method flux spikes up to almost 0.4 Nm^{-2} on the 21st of April, while the sonic anemometer measured only a bit over 0.2 Nm^{-2} at the same time. Smallest values are observed on the 20th and 22nd of April, when the flux stays below 0.1 Nm^{-2}. The magnitude of the flux matches well with the observed wind speed (see Figure 6.3) with the highest values reached during stronger wind speeds. The correlation coefficient between the momentum flux and wind speed was 0.86. No diurnal cycle could be found.

The profile and the direct measurements of the sensible heat flux match well in sign but poorly in magnitude. The best match is found on the 21st of April. At other times, the gradient method mostly gives a much larger flux. The sonic anemometer measured values from -50 Wm^{-2} to +10 Wm^{-2} while the gradient method gives a much wider range of values, from -70 Wm^{-2} to +60 Wm^{-2} or even more. When comparing with the observed stability (Figure 6.4), it can be

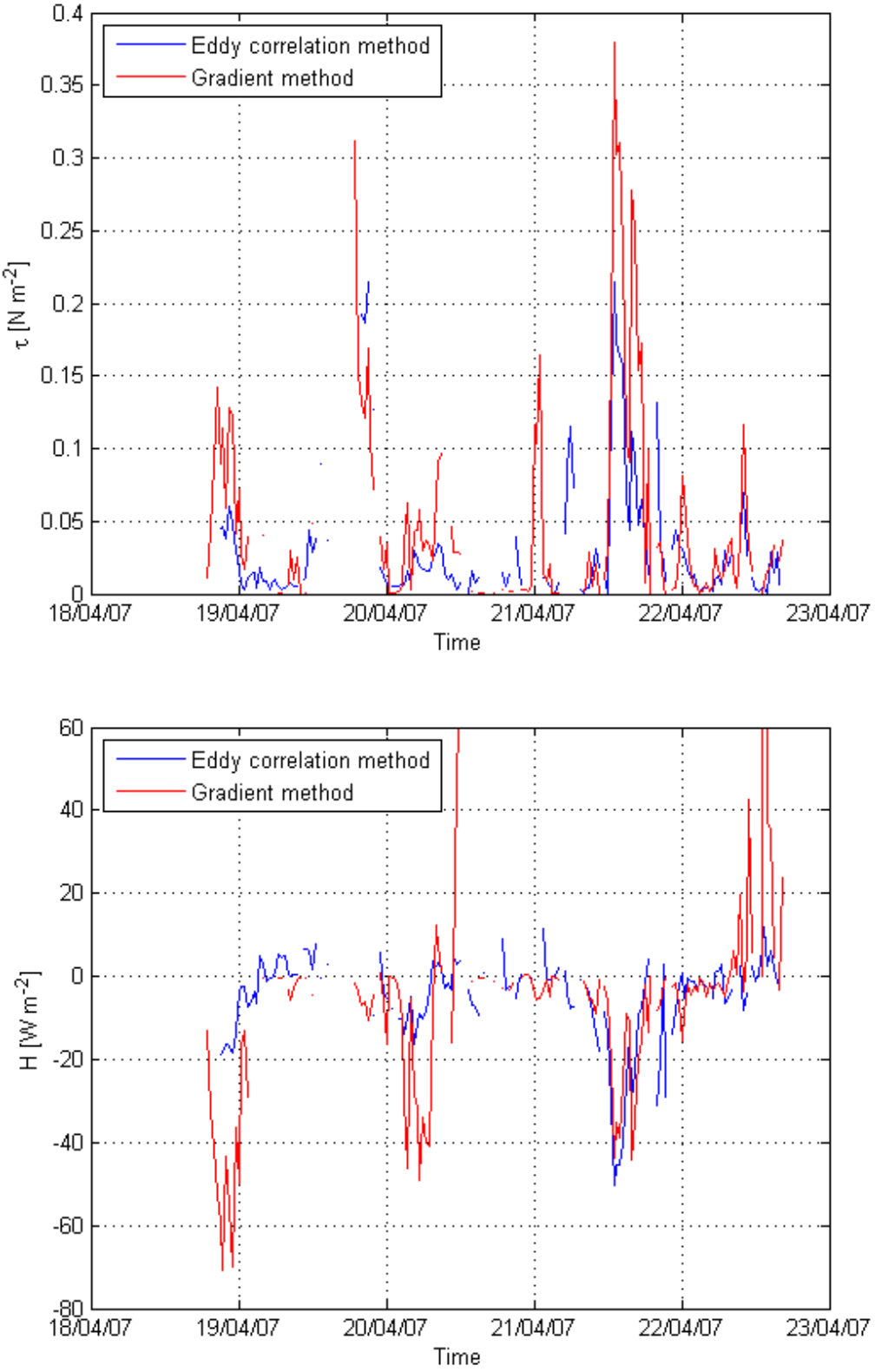

Figure 6.14: *Time series of the turbulent fluxes of momentum τ and sensible heat H measured in Wahlenbergfjorden in April 2007.*

seen that an upward heat flux occurs when the atmosphere is unstable, while a downward heat flux is observed during stable periods. No diurnal variation is visible in the time series.

6.6 Integral turbulence characteristics

The integral turbulence characteristics can be used for a data quality test (Foken and Wichura, 1996). This method is based on the assumption that the standard deviations of the wind speed components normalized by the friction velocity and the standard deviation of temperature normalized by corresponding temperature scale are some unique functions of the stability parameter z/L.

In this case, the following empirical formula was tested for wind speed (Arya, 2001):

$$\frac{\sigma_w}{u_*} = 1.25[1 - 3(z/L)]^{1/3} \tag{6.1}$$

where σ_w is the standard deviation of vertical wind speed. This formula can only be used for unstable stratification. There was significant scatter in the scaled wind speed variance, but no strange features occurred (not shown here). Thus, we can assume that the wind speed measurements by the sonic are rather reliable.

For temperature, the following formula was applied (Wyngaard et al., 1971)

$$(\frac{\sigma_\theta}{\theta_*})^2 = 0.95[-(z/L)]^{-(2/3)} \tag{6.2}$$

where σ_θ is the standard deviation of potential temperature. This formula is also only suitable for unstable stratification.

It was found that the scaled temperature variance did not behave as expected by the formula (not shown here). The deviations from the prediction were larger in 2006 than in 2007. When applying a criteria of $|\overline{w'\theta'}| > 0.005$ and $\sigma_\theta > 0.04$, which can be expected to be the resolution of the measurements, a majority of the values did not fulfill these criteria. However, the values that did follow the criteria, were much closer to expected values. This leads to the conclusion that the measured heat flux was too small. Some of the fluctuations were probably too small for the resolution of the sonic anemometer and thus errors were large. This affects all the calculations which include the heat flux, for example stability parameter and sensible heat flux calculations.

6.7 Stability functions

According to the Monin-Obukhov similarity theory, in the surface layer the non-dimensional gradients of wind speed (Eq. 2.5) and temperature (Eq. 2.6) must be related to the stability, expressed by z/L. The non-dimensional gradient of wind speed ϕ_m plotted against stability for 2006 is presented in Figure 6.15. The solid curve represents the predicted similarity functions according to Equation 2.7 for unstable region and Equation 2.8 for stable region. Most of the values are in the near-neutral range and follow the theory quite well. The values in the unstable region show some scatter.

The estimated non-dimensional gradient of temperature is not presented here, since the results were obviously wrong. The sign of the stability parameter from the sonic measurements was opposite to that from the weather mast measurements almost during half of the time. This caused all the values of ϕ_h for stable stratification to be negative.

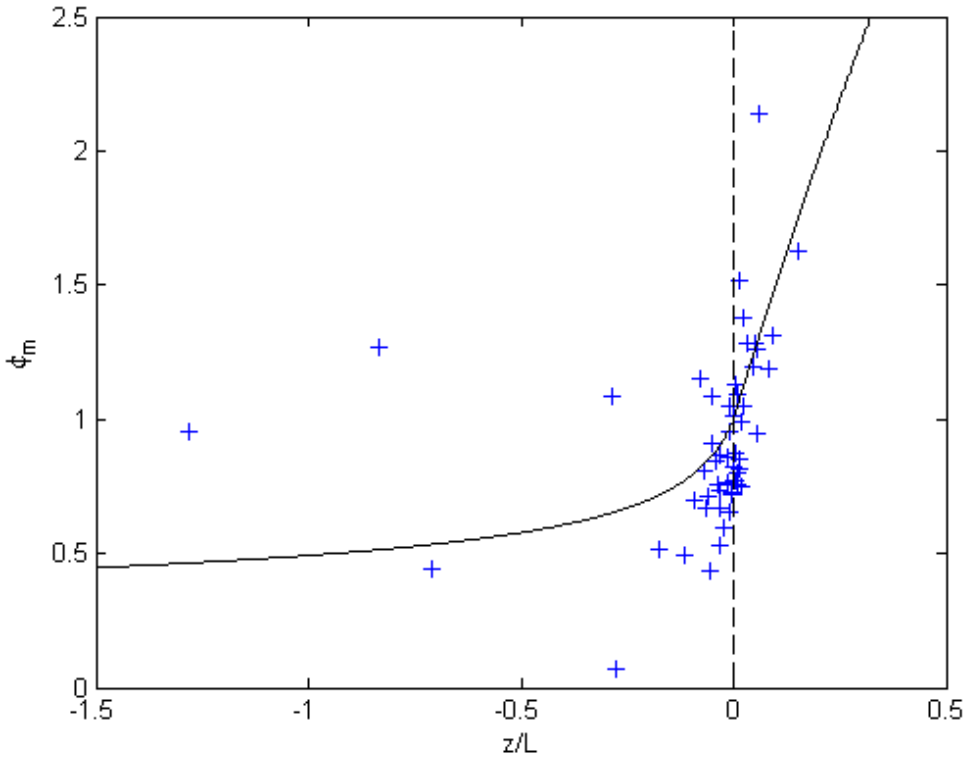

Figure 6.15: *The non-dimensional gradient of wind speed ϕ_m as a function of stability for 2006.*

The non-dimensional gradient of wind speed as a function of stability for 2007 is presented in Figure 6.16. The calculated stability function ϕ_m seems to follow the predicted functions quite well in the near-neutral region. The unstable region and slightly stable region show more scatter, but on average the values follow the prediction. In the very stable region the values fall below the predicted curve, and the scatter becomes larger as the stability increases.

A similar plot for the non-dimensional temperature gradient ϕ_h for 2007 is presented in Figure 6.17 (note the different scale to Figure 6.16). The results are much more scattered than those obtained for ϕ_m. The largest scatter is observed in the near-neutral range. The stable region values seem to be much smaller than predicted by the curve by Holtslag and De Bruin (1988). The values do not seem to increase with increasing stability as expected but tend to level off. The plot shows quite many negative values of ϕ_h which indicate that the stability calculated from the sonic anemometer measurements was of different sign than the stability calculated from the profile measurements.

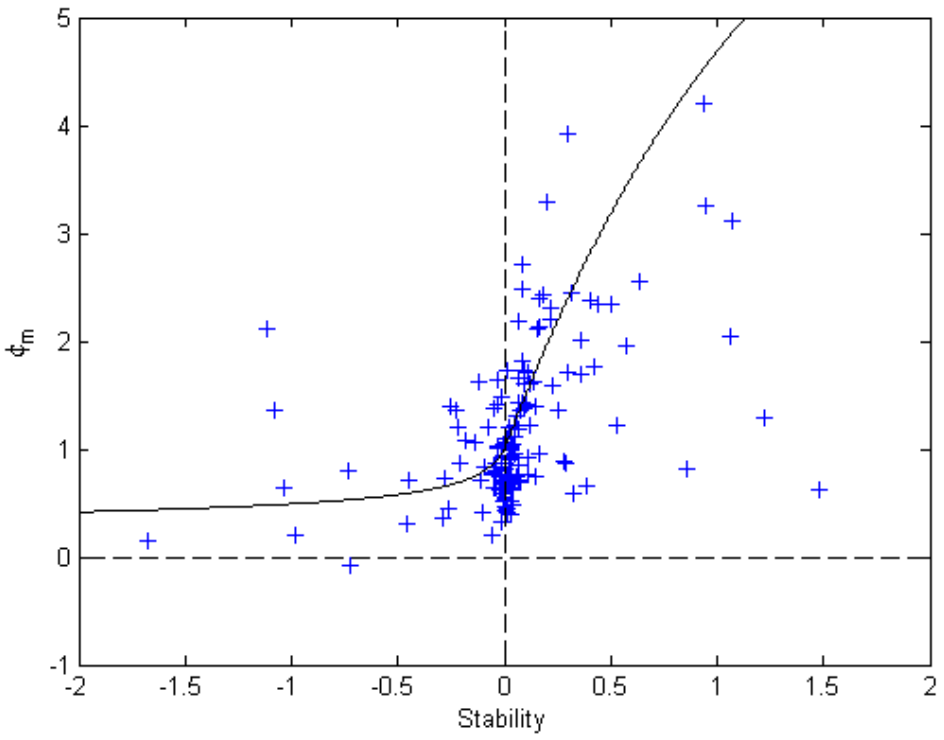

Figure 6.16: *The non-dimensional gradient of wind speed ϕ_m as a function of stability for 2007.*

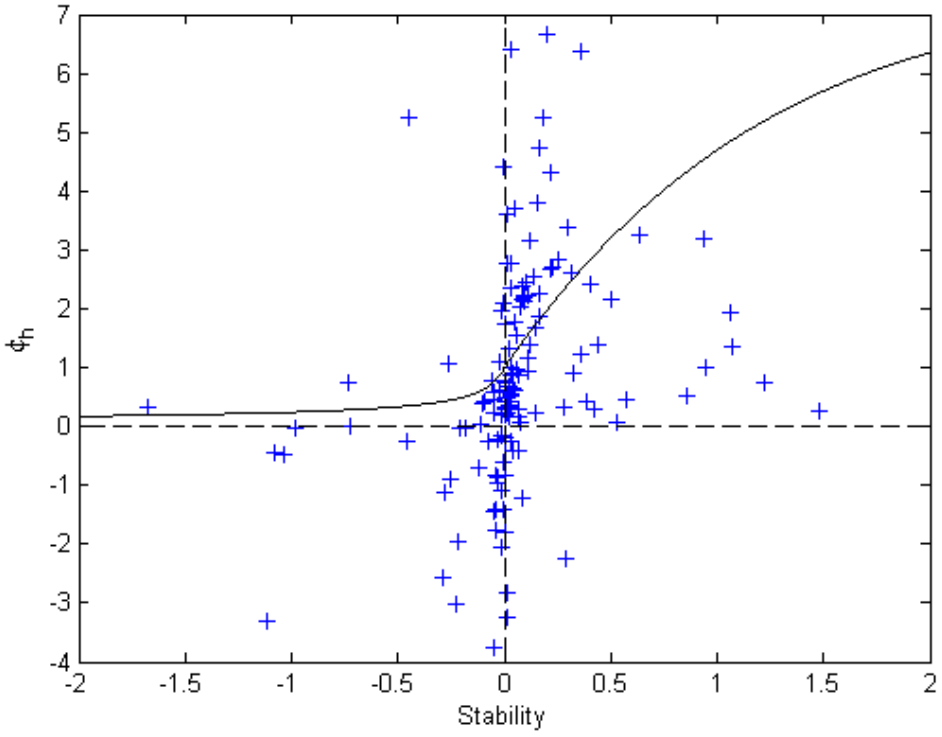

Figure 6.17: *The non-dimensional gradient of temperature ϕ_h as a function of stability for 2007.*

7 Discussion

The data presented in this study cover a relatively short time period. Therefore, the results are essentially affected by the synoptic scale situation. Hence, the results cannot be generalised, but some aspects are presented in this chapter. Some issues concerning the measurement and calculation of the turbulent fluxes are addressed. The non-dimensional gradients are used to investigate the validity of the Monin-Obukhov similarity theory and possible error sources for the measurements are evaluated.

7.1 Flux measurement issues

The time scale over which the means and deviations are calculated must be appropriately chosen. The calculated flux depends on the averaging timescale, since all scales of motion up to the averaging timescale are included in the flux (Vickers and Mahrt, 2003). Too short a timescale produces underestimated fluxes, while choosing too long a time scale will contaminate the fluxes with mesoscale fluctuations and possible gravity waves. The separation between turbulence and mesoscale motions becomes critical with weak turbulence, since failure to remove even a small fraction of the mesoscale motion from the weak turbulence signal can lead to serious contamination of the estimated turbulent fluxes and to large random flux errors. Intermittent turbulence may cause problems in the averaging process and produce erroneous covariances, which in turn lead to erroneous fluxes. The averaging time may be chosen depending on the goal of the research. In similarity relatioship studies, it is attempted to remove all nonturbulent contributions, while in surface energy budget studies also heat fluxes at larger timescales may be included (Vickers and Mahrt, 2003). For example in SHEBA, a one hour averaging time was chosen (Persson et al., 2002; Grachev et al., 2007). This probably includes all contributions to the fluxes. A typical value for the averaging time is 30 minutes, which has commonly been used in boundary layer studies (e.g.

Forrer and Rotach, 1997; Brümmer et al., 2002). It was also chosen for this study. However, in very stable situations some mesoscale influence may have entered the fluxes.

Flux loss may occur due to temporal resolution. When the resolution of the data cannot resolve the smallest transporting eddies, the flux calculated from the data probably underestimates the true flux. Resolution problems can result e.g. from the sampling rate. The sonic anemometer had a different sampling rate in 2007 and in 2006. The lower sampling rate of 10 Hz in 2006 may have resulted in fluxes that were too small. This conclusion is in agreement with Howell and Sun (1999), who found indications that the eddy correlation sampled at 10 Hz may underestimate the heat flux due to the missed contribution from very small eddies. Thus, the eddy correlation fluxes were probably underestimated when using the sampling rate of 10 Hz.

The chosen similarity functions affect the stability corrections and therefore also the fluxes calculated from profile measurements. As seen from Figures 6.16 and 6.17, even the functions by Holtslag and De Bruin (1988) seem to overestimate the gradient functions in stable conditions. If the gradient functions are overestimated, as happens for strong stability, then u_* and θ_* are underestimated as are also the fluxes calculated from them. According to this, the fluxes obtained from the gradient method were underestimated in stable conditions. The gradient method gave larger fluxes than the eddy correlation method. The reason may be that topographic effects are more important for profiles than turbulent mixing. Also, it was found that variation of the fluxes within the instrument accuracies may be large, on the order of 30 to 60 %. These estimations were done by recalculating the fluxes from the biggest and smallest possible gradients obtained according to the instrument accuracies. The gradients were calculated separately for wind speed and temperature. The sensible heat flux was mainly dependent on the temperature gradient, while the momentum flux depended on both temperature and wind speed gradients. The errors were found to be larger in 2006, when the gradients were smaller than in 2007.

7.2 The validity of the Monin-Obukhov theory

The Monin-Obukhov similarity theory is the cornerstone of our knowledge of the atmospheric surface layer. However, there are several limitations with the theory. In order to apply the Monin-Obukhov similarity theory, many assumptions

have to be made. The theory presumes horizontal homogeneity and stationarity in order to be valid. Clearly, that is always not the case in a fjord, where the requirement of horizontal homogeneity is not fulfilled, at least not for cross-fjord wind directions. However, the along-fjord direction may meet this requirement. Also the influences of nonstationarity may violate the requirements. Nonstationary conditions most often occur with weak large-scale flow and significant mesoscale variability (Vickers and Mahrt, 1997). In 2006 the large-scale flow controlled the wind field, while in 2007 the large-scale flow was weak and mesoscale motions played a bigger role. Thus, nonstationary conditions were likely to exist in 2007 and affect the validity of the Monin-Obukhov similarity theory.

Traditional Monin-Obukhov similarity theory works well in a weakly stable boundary layer. The very stable boundary layer is characterised by weak, intermittent turbulence even near the surface, and it has been suggested that the similarity theory breaks down (Mahrt, 1999).

If the fluxes at level z significantly differ from their surface values, Monin-Obukhov similarity does not apply anymore and local similarity should be used instead. In local similarity, local values of fluxes are used instead of the surface values. If the surface layer is shallow, the surface fluxes are no longer appropriate scaling parameters and their local values should be used instead. In many studies, the surface layer in stable cases has been found to be very shallow, less than 10 meters (Forrer and Rotach, 1997; Howell and Sun, 1999). Furthermore, in the presence of a katabatic flow the surface layer height may even be less than three meters (Van Der Avoird and Duynkerke, 1999). Both of these situations may have occurred in Wahlenbergfjorden and resulted in the invalidity of the surface scaling by the Monin-Obukhov similarity theory. Even if no signs of katabatic flow were found from the wind direction, temperature and humidity measurements of the big weather mast, effects of katabatic winds may still be present in turbulent flow.

7.2.1 The non-dimensional gradients ϕ_m and ϕ_h

The accuracy of the non-dimensional gradients ϕ_m and ϕ_h depends on the chosen similarity functions. The uncertainty in the nondimensional gradient functions is still large in stable conditions, as can be seen from Figure 2.2. Mahrt (1999) relates this uncertainty to the following possibilities. The influence of individual roughness elements are more pronounced with strong stability, and the vertical divergence of the flux cannot be neglected. Thus, traditional surface layer does not

exist. Another option is that the surface layer exists but is below the observational level. Thirdly, the fluxes and stability functions may be impossible to determine due to instrumental and flux sampling problems in weak intermittent turbulence. In this study, the equations from Holtslag and De Bruin (1988) were chosen for stable atmosphere, since it is nowadays well known that traditional linear relationships overestimate ϕ_m and ϕ_h for large ζ. The equations by Holtslag and De Bruin are also suitable for use over snow and ice. Lately, these equations have been widely used for describing stability effects in very stable stratification. However, according to Wahlenbergfjorden data, both stability functions increase more slowly than predicted by these equations. The deviation from the theoretical curves was largest in strongly stable cases.

Both Forrer and Rotach (1997) and Howell and Sun (1999) found that the estimated ϕ_h levels off around $z/L = 0.5$. This can also be seen in the results in Figure 6.17, but the scatter is large and there are only a few data points.

The differences between the model functions ϕ_m and ϕ_h and the observations may be at least partly caused by snow drift. Additionally, during snow drift, the cup anemometers tend to measure too low a wind speed in the lowest levels due to deposition of snow on the cups (Handorf et al., 1999). Some positive $\overline{u'w'}$ covariance values were measured. They indicate a moving surface and snow drift may be the cause for these values. 11 % of the $\overline{u'w'}$ covariance values were positive in 2007, only 2 % in 2006. This may explain the larger deviation from the theory in 2007.

7.2.2 Self-correlation

Self-correlation arises when one group of variables is plotted against another, and the two groups under consideration have one or more common variables. Then a part of the correlation is caused by artificial, mathematical reasons (Baas et al., 2006). Self-correlation is a serious problem, and the success of the similarity theory could have been previously overestimated (Mahrt, 1999).

The non-dimensional gradients of ϕ_m and ϕ_h are traditionally plotted against stability parameter z/L. The problem is that the same variables, primarily u_*, appear in the definitions of ϕ_m, ϕ_h and z/L (see Equations 2.2, 2.5 and 2.6). Therefore, there is a self-correlation in the analyses for ϕ_m and ϕ_h versus z/L. The degree of scatter is different for ϕ_m and ϕ_h, which is a result of self-correlation (Baas et al., 2006). In stable regions, ϕ_h will always show a larger scatter.

Scaling based on the gradient or bulk Richardson number has been suggested to avoid the self-correlation problem (Baas et al., 2006; Grachev et al., 2007). If the Richardson number is used as a stability parameter, figures of gradient functions plotted against stability would suffer less from self-correlation. There is still some self-correlation, since the vertical gradient of wind speed is a shared variable, but it is smaller compared to using ζ.

7.3 Data quality and error sources

First of all, it has to be remembered that the measurement campaigns presented in this study were done in learning purposes as a part of university courses. Many people, possibly with no previous experience in such field work, were involved in making the measurements and in taking notes, which may have resulted in human errors.

According to Foken and Wichura (1996) the reasons for error in direct eddy correlation measurements can be divided into three groups; deviations from the theoretical requirements, problems of the sensor configuration and meteorological problems.

Deviations from the theoretical requirements mainly address the requirements of the Monin-Obukhov similarity theory. Horizontal inhomogeneity and nonstationarity, affecting the validity of the Monin-Obukhov similarity theory, may have been a factor for inaccurate flux estimates.

Sensor configuration problems may be related to flow distortion, measuring height or tilt error. For the measurements presented in this study, flow distortion was taken care of by removing data collected during disturbed wind directions. Measuring height was checked to fill the requirements and recommendations by Kaimal and Finnigan (1994). Tilt error was also corrected.

Meteorological problems may include internal boundary layers, variation in surface layer height, gravity waves in inversion situations or lack of turbulence (Foken and Wichura, 1996). Internal boundary layer may have occurred when the wind was blowing across the ice edge. When winds were blowing across the shoreline with changing roughness, internal boundary layers may have also occurred. Surface layer height might have been lower than the measurement height, especially in stably stratified conditions or in the presence of a katabatic wind. Some katabatic flow situations were probably present and in those situations the observed fluxes were smaller than their surface values. This was not accounted

for in the calculations. The values of the stability parameter were occasionally very high, indicating that turbulence was lacking at least part of the time.

The eddy correlation method is thought to be the most reliable method in determining turbulent fluxes, and is often used as a reference method. However, the eddy correlation measurements presented in this study may have been inaccurate due to the above mentioned reasons.

Same problems as in sonic anemometer measurements may cause error in also profile measurements. The profile measurement were made at one minute intervals, which makes the measurements less accurate. Inaccuracy of the instruments may have caused error. The errors are larger in situations when the measured quantities are small. The gradient method is very sensitive to the differences between the two measuring levels, which may have caused large errors in the calculations. The method is sensitive to errors at each measurement height as well. In many cases, the differences of wind speed and temperature between the two levels were small, and thus the measurements of the gradients were liable to errors. Also very low wind speeds may result in inaccurate flux calculations when using the gradient method.

The cup anemometers have a tendency to overspeed, which causes an error of about 5% to 10% (Kaimal and Finnigan, 1994). In this study the measurements were not corrected for overspeeding, since mainly only gradients are used for calculations.

In 2007, the small mast 2 wind direction showed a clear bias, which was corrected for. However, not knowing the reason for this bias, the results from this mast (Figures 6.9(c), 6.10(e) and (f)) should be interpreted with special caution.

The weather masts were deployed on land-fast sea ice, which makes the platform quite difficult for accurate and stable deployment of the instruments. It is very likely that some movement of the masts occurred during high winds. The sonic anemometer measurements are more liable to errors caused by the movement than profile measurements, since the sonic anemometer measures all three wind components.

8 Conclusions

During scientific cruises to Wahlenbergfjorden in the spring of 2006 and 2007, a wide range of meteorological data was collected from the atmospheric boundary layer. A fast response three-dimensional sonic anemometer was used to measure turbulent fluxes. Wind speed, temperature and humidity were observed at several levels with profile masts in various locations.

The turbulent fluxes of momentum and sensible heat were calculated using two methods, the eddy correlation method and the gradient method. Usually the eddy correlation method is used as the reference method. In this study, both of the methods were found to be prone to errors. The eddy correlation method errors resulted from resolution problems, small fluxes and possible nonstationarity due to mesoscale motions. The instrument resolution may not have been good enough to capture some of the smallest fluctuations. Especially the temperature measurements were found to be sensitive to errors. In 2007, many positive values of $\overline{u'w'}$ covariance were measured by the sonic anemometer. This indicated a moving surface, which may be connected to drifting or blowing snow. The gradient method is dependent on the accuracy of the gradient measurement. Due to small fluxes and instrument accuracies, the errors when using this method were found to be large. Also possible violations of the Monin-Obukhov similarity theory affect the results.

The eddy correlation method and the gradient method gave quite similar results for fluxes in 2006, while in 2007 the gradient method usually gave larger fluxes. The results of the gradient method are affected by the choise of similarity functions, but even the chosen similarity functions seemed to underestimate the turbulent mixing. Fluxes from both the eddy correlation method and gradient method were possibly underestimated.

The non-dimensional gradients of wind speed and temperature were found to have a lot of scatter especially for larger stabilities. The values had a tendency to level off when stability increased. This indicates that large background turbulence

was present.

The validity of the Monin-Obukhov theory can be questioned for cross-fjord winds since the requirement of horizontal homogeneity is not fulfilled. For along-fjord wind directions the theory may be valid, but only if surface-layer scaling can be used. This may not be the case in very stable situations or when katabatic winds are present, since in these cases the surface layer height can be less than the measurement heights. The requirement of stationarity was probably met in 2006, but in 2007 the mesoscale variability was larger and probably resulted in unstationary conditions from time to time.

There were clear indications that the near-surface wind field is modified by local topography, resulting in e.g. channelling effects and gravity-driven drainage flows. In case of a strong large-scale flow, the effects of topography were found to be weaker.

The surface roughness had a large scatter. However, the values for roughness length were mostly typical for a snow-covered ice, on the order of $10^{-3}m$ to $10^{-4}m$. The roughness length values for wind directions along the fjord axis were found to be significantly smaller than those for cross-fjord wind directions. The roughness length was found to be weakly dependent on wind speed, possibly due to drifting or blowing snow.

Bibliography

Andreas, E. L. (1998). *The Atmospheric Boundary Layer Over Polar Marine Surfaces,* in: Leppäranta, M. (ed.), Physics of ice-covered seas, Volume 2, pp. 715–773. Helsinki University Printing House.

Andreas, E. L. (2002). Parameterizing Scalar Transfer over Snow and Ice: A Review. *Journal of Hydrometeorology 3*(4), 417–432.

Andreas, E. L., R. E. Jordan, and A. P. Makshtas (2005). Parameterizing turbulent exchange over sea ice: the ice station Weddell results. *Boundary-Layer Meteorology 114*(2), 439–460.

Argentini, S., G. Mastrantonio, A. Maurizi, T. Georgiadis, and M. Nardino (2003). Characteristics of the boundary layer at Ny-Ålesund in the Arctic during the ARTIST field experiment. *Annals of Geophysics 46*(2), 185–195.

Arya, S. P. (2001). *Introduction to Micrometeorology.* Academic Press.

Baas, P., G. J. Steeneveld, B. J. H. van de Wiel, and A. A. M. Holtslag (2006). Exploring Self-Correlation in Flux–Gradient Relationships for Stably Stratified Conditions. *Journal of the Atmospheric Sciences 63*(11), 3045–3054.

Beljaars, A. C. M. and A. A. M. Holtslag (1991). Flux Parameterization over Land Surfaces for Atmospheric Models. *Journal of Applied Meteorology 30*(3), 327–341.

Brümmer, B., D. Schröder, J. Launiainen, T. Vihma, A. S. Smedman, and M. Magnusson (2002). Temporal and spatial variability of surface fluxes over the ice edge zone in the northern Baltic Sea. *Journal of Geophysical Research (Oceans 107*(C8), 11–1.

Brümmer, B. and S. Thiemann (2002). The Atmospheric Boundary Layer In

An Arctic Wintertime On-Ice Air Flow. *Boundary-Layer Meteorology 104*(1), 53–72.

Businger, J. A., J. C. Wyngaard, Y. Izumi, and E. F. Bradley (1971). Flux-Profile Relationships in the Atmospheric Surface Layer. *Journal of the Atmospheric Sciences 28*(2), 181–189.

Campbell Scientific (1998). *CSAT3 Three Dimensional Sonic Anemometer Instruction Manual*. Campbell Scientific.

Foken, T. and B. Wichura (1996). Tools for quality assessment of surface-based flux measurements. *Agricultural and Forest Meteorology 78*(1-2), 83–105.

Forrer, J. and M. W. Rotach (1997). On the turbulence structure in the stable boundary layer over the Greenland ice sheet. *Boundary-Layer Meteorology 85*(1), 111–136.

Grachev, A. A., E. L. Andreas, C. W. Fairall, P. S. Guest, and P. O. G. Persson (2007). SHEBA flux–profile relationships in the stable atmospheric boundary layer. *Boundary-Layer Meteorology 124*(3), 315–333.

Handorf, D., T. Foken, and C. Kottmeier (1999). The stable atmospheric boundary layer over an antarctic ice sheet. *Boundary-Layer Meteorology 91*(2), 165–189.

Hartmann, J., F. Albers, S. Argentini, A. Bochert, U. Bonafe, W. Cohrs, A. Conidi, D. Freese, T. Georgiadis, A. Ippoliti, et al. (1999). Arctic Radiation and Turbulence Interaction Study (ARTIST). *Rep. Polar Res 305*.

Högström, U. (1988). Non-dimensional wind and temperature profiles in the atmospheric surface layer: A re-evaluation. *Boundary-Layer Meteorology 42*(1), 55–78.

Holtslag, A. A. M. and H. A. R. De Bruin (1988). Applied Modeling of the Nighttime Surface Energy Balance over Land. *Journal of Applied Meteorology 27*(6), 689–704.

Howell, J. F. and J. Sun (1999). Surface-Layer Fluxes in Stable Conditions. *Boundary-Layer Meteorology 90*(3), 495–520.

Jordan, R. E., E. L. Andreas, and A. P. Makshtas (1999). Heat budget of snow-covered sea ice at North Pole 4. *Journal of Geophysical Research. C. Oceans 104*, 7785–7806.

Kaimal, J. C. and J. J. Finnigan (1994). *Atmospheric Boundary Layer Flows: Their Structure and Measurement.* Oxford University Press, USA.

Kaimal, J. C. and J. E. Gaynor (1991). Another look at sonic thermometry. *Boundary-Layer Meteorology 56*(4), 401–410.

Launiainen, J. and T. Vihma (1990). Derivation of turbulent surface fluxes–an iterative flux-profile method allowing arbitrary observing heights. *Environmental Software 5*(3), 113–124.

Lee, X., J. Finnigan, and K. T. Paw U (2004). *Coordinate systems and flux bias error,* in: Lee, X., W. J. Massman and B. E. Law (eds.), Handbook Of Micrometeorology: A Guide For Surface Flux Measurement And Analysis, pp. 33–66. Kluwer Academic Publishers.

Liu, H., G. Peters, and T. Foken (2001). New Equations For Sonic Temperature Variance And Buoyancy Heat Flux With An Omnidirectional Sonic Anemometer. *Boundary-Layer Meteorology 100*(3), 459–468.

Lumley, J. L. and H. A. Panofsky (1964). The Structure of Atmospheric Turbulence. *239pp. Wiley, New York 226.*

Mahrt, L. (1999). Stratified Atmospheric Boundary Layers. *Boundary-Layer Meteorology 90*(3), 375–396.

Monin, A. S. and A. M. Obukhov (1954). Basic regularity in turbulent mixing in the surface layer of the atmosphere. *Akad. Nauk. SSSR Trud. Geofiz. Inst 24*, 163–187.

Olsson, P. Q. and J. Y. Harrington (2000). Dynamics and energetics of the cloudy boundary layer in simulations of off-ice flow in the marginal ice zone. *Journal of Geophysical Research 105*, 11.

Paulson, C. A. (1970). The Mathematical Representation of Wind Speed and Temperature Profiles in the Unstable Atmospheric Surface Layer. *Journal of Applied Meteorology 9*(6), 857–861.

Persson, P. O. G., C. W. Fairall, E. L. Andreas, P. S. Guest, and D. K. Perovich (2002). Measurements near the Atmospheric Surface Flux Group tower at SHEBA: Near-surface conditions and surface energy budget. *J. Geophys. Res 107*(C10), 10–1029.

Serreze, M. C., J. D. Kahl, and R. C. Schnell (1992). Low-Level Temperature Inversions of the Eurasian Arctic and Comparisons with Soviet Drifting Station Data. *Journal of Climate 5*(6), 615–629.

Stull, R. B. (1988). *An Introduction to Boundary Layer Meteorology*. Kluwer Academic Publishers.

Svendsen, H., A. Beszczynska-Moller, J. O. Hagen, B. Lefauconnier, V. Tverberg, S. Gerland, J. B. Orbok, K. Bischof, C. Papucci, M. Zajaczkowski, R. Azzolini, O. Bruland, C. Wiencke, J.-G. Winther, and W. Dallmann (2002). The physical environment of Kongsfjorden-Krossfjorden, an Arctic fjord system in Svalbard. *Polar Research 21*(1), 133–166.

Uttal, T., J. A. Curry, M. G. Mcphee, D. K. Perovich, R. E. Moritz, J. A. Maslanik, P. S. Guest, H. L. Stern, J. A. Moore, R. Turenne, A. Heiberg, M. C. Serreze, D. P. Wylie, O. G. Persson, C. A. Paulson, C. Halle, J. H. Morison, P. A. Wheeler, A. Makshtas, H. Welch, M. D. Shupe, J. M. Intrieri, K. Stamnes, R. W. Lindsey, R. Pinkel, W. S. Pegau, T. P. Stanton, and T. C. Grenfeld (2002). Surface Heat Budget of the Arctic Ocean. *Bulletin of the American Meteorological Society 83*(2), 255–276.

Van Der Avoird, E. and P. Duynkerke (1999). Turbulence in a Katabatic Flow. *Boundary-Layer Meteorology 92*(1), 37–63.

Vickers, D. and L. Mahrt (1997). Quality Control and Flux Sampling Problems for Tower and Aircraft Data. *Journal of Atmospheric and Oceanic Technology 14*(3), 512–526.

Vickers, D. and L. Mahrt (2003). The Cospectral Gap and Turbulent Flux Calculations. *Journal of Atmospheric and Oceanic Technology 20*(5), 660–672.

Vihma, T. (2005). Preface. *Boundary-Layer Meteorology 117*(1), 1–4.

Vihma, T., J. Hartmann, and C. Lüpkes (2003). A Case Study Of An On-Ice Air Flow Over The Arctic Marginal Sea-Ice Zone. *Boundary-Layer Meteorology 107*(1), 189–217.

Whiteman, C. (2000). *Mountain Meteorology: Fundamentals and Applications*. Oxford University Press, USA.

Wilczak, J. M., S. P. Oncley, and S. A. Stage (2001). Sonic Anemometer Tilt Correction Algorithms. *Boundary-Layer Meteorology 99*(1), 127–150.

Wyngaard, J. C., O. R. Coté, and Y. Izumi (1971). Local Free Convection, Similarity, and the Budgets of Shear Stress and Heat Flux. *Journal of the Atmospheric Sciences 28*(7), 1171–1182.

Zilitinkevich, S. S., I. Mammarella, A. A. Baklanov, and S. M. Joffre (2008). The Effect of Stratification on the Aerodynamic Roughness Length and Displacement Height. *Boundary-Layer Meteorology 129*, 179–190.

REPORT SERIES IN GEOPHYSICS
(Reports 1 to 25 are listed up to Report No 51)

26. Simojoki, H., 1992: Geofysiikan tulo oppiaineeksi Helsingin yliopistossa (2nd ed.).
27. Leppäranta, M., Haapala, J. (eds.), 1993: Proceedings of the first workshop on the Baltic sea ice climate, Tvärminne, Finland, 22-26 August 1993.
28. Vihma, T. (ed.), 1994: Evening sessions of the summer school on physics of ice-covered seas, Savonlinna, Finland, 6-17 June 1994.
29. Pulkkinen, K., 1995: STD-12 mini-CTD:n käyttö ja datan kalibrointi (English summary: The use of STD-12 mini-CTD and calibration of data).
30. Pulkkinen, K. (ed.), 1995: Underwater optical measurements made during the first concentrated field effort (CFE 1) of NOPEX - A data report.
31. Multala, J., Hautaniemi, H., Oksama, M., Leppäranta, M., Haapala, J., Herlevi, A., Riska, K., Lensu, M., 1995: Airborne electromagnetic surveying of Baltic sea ice.
32. Pulkkinen, K. (ed.), 1995: Proceedings of the 2nd Finnish-Estonian seminar on underwater optics with applications, Helsinki, 10-12 April 1995.
33. Launiainen, J., Cheng, B., 1995: A simple non-iterative algorithm for calculating turbulent bulk fluxes in diabatic conditions over water, snow/ice and ground surface.
34. Stipa, T., 1996: Water renewal and vertical circulation of Pohja Bay.
35. Haapala, J., Alenius, P., Dubra, J., Klyachkin, S.V., Kõuts, T., Leppäranta, M., Omstedt, A., Pakstys, L., Schmelzer, N., Schrum, C., Seinä, A., Strübing, K., Sztobryn, M., Zaharchenko, E., 1996: IDA. Ice data bank for Baltic Sea climate studies.
36. Leppäranta, M. (ed.), 1996: AISA lake experiment 1993-94. Final Report.
37. Haapala, J., Leppäranta, M. (eds.), 1997: ZIP-97 data report.
38. Pulkkinen, K. (ed.), 1998: Proceedings of the 4th Finnish-Estonian seminar on underwater optics with applications, Lammi, 22-24 April 1997.
39. Saloranta, T.M., 1998: Snow and snow ice in sea ice thermodynamic modelling.
40. Leppäranta, M. (ed.), 1998: Downscaling in sea ice geophysics.
41. Herlevi, A. (ed.), 1999: The optics ground truth of the Finnish SALMON experiment.
42. Haapala, J., 2000: Modelling of the seasonal ice cover of the Baltic sea.
43. Zhang, Z., 2000: On modelling ice dynamics of semi-enclosed seasonally ice-covered seas.
44. Jevrejeva S., Drabkin, V.V., Kostjukov, J., Lebedev, A.A., Leppäranta, M., Mironov, Ye. U., Schmelzer, N., Sztobryn, M., 2002: Ice time series of the Baltic Sea.
45. Herlevi, A., 2002: Inherent and apparent optical properties in relation to water quality in Nordic waters.
46. Leppäranta, M. (ed.), 2003, Proceedings of the seminar “Sea Ice Climate and Marine Environments in the Okhotsk and Baltic Seas – The Present Status and Prospects”.
47. Rasmus, K., Granberg, H., Kanto, K., Kärkäs, E., Lavoie, C., Leppäranta, M., 2003: Seasonal snow in Antarctica data report.
48. Rasmus, S., 2005: Snow pack structure characteristics in Finland – Measurements and modelling.
49. Kanto, E., 2006: Snow characteristics in Dronning Maud Land, Antarctica.
50. Halkola, K., 2006: The orographic climate factors contributing to the mass balance of small glaciers in North-Iceland.
51. Elo, A.-R., 2007: Effects of climate and morphology on temperature conditions of lakes.
52. Donadini, F., 2007: Features of the geomagnetic field during the Holocene and Proterozoic.
53. Wang, K., 2007: On the mechanical behaviour of compacted pack ice: Theoretical and numerical investigations.
54. Koistinen, E., 2007: Antarktikan ilmastohistoria.
55. Kanto, E., Leppäranta, M., Mattila, O.-P., 2008: Seasonal snow in Antarctica. Data report II.
56. Oikkonen, A.., 2008: Variability and changes of Arctic sea ice cover, 1975-2000.
57. Forsström, S., 2008:Carbonaceous aerosol particles in Svalbard snow.

ISBN 978-952-10-4229-4 (printed version)
ISBN 978-952-10-4230-0 (pdf-version)
ISSN 0355-8630

Helsinki 2009
Yliopistopaino